5 From Fundamentals to Applications – Quantum Electrodynamics, Strong Fields, Ion-Matter Interactions

Overview

• **Relativistic atomic-collision dynamics in the strongest electromagnetic fields** (Chapter 5.1.2.1). There, the focus will be on the various electronic transitions in relativistic heavy-ion collisions, dynamically induced many-electron processes – as well as the spectroscopy of the quasi-molecular 1sσ orbital – in critical and supercritical fields. In close ion-atom collisions, the critical field strength, where spontaneous e^+-e^--pair creation becomes possible, can be probed for the first time under well defined conditions with respect to charge state and energy of the ion with a luminosity sufficient for an unambiguous detection. In a H-like uranium ion the 1s electron probes to some extent those critical fields (Figure 5.1)

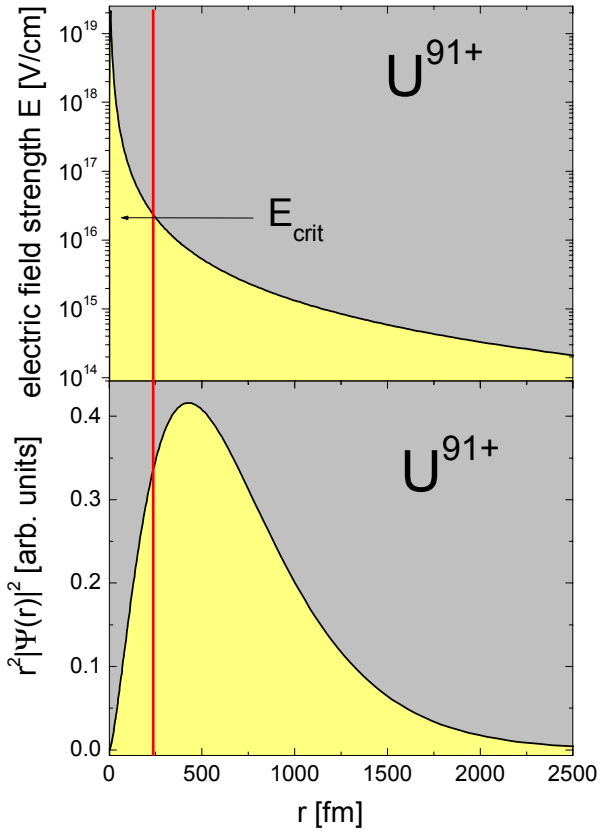

Figure 5.1: Radial 1s electron density in H-like uranium vs. distance from the nuclear center (bottom), together with the electric field strength probed by the electron. Also marked is the 'critical' field strength at about 250 fm, where spontaneous e^+-e^- pair creation becomes possible.

In the recent past accelerator-based atomic physics has advanced into hitherto unexplored areas of research, encompassing high energies, high atomic charge states and strong electromagnetic fields. First tentative benchmarks were set by the heavy-ion storage cooler rings, in particular by the experimental storage ring ESR at GSI,

via precision spectroscopy of relativistic few-electron ions, and via the exploration of the interaction of relativistic ions with atoms, electrons and photons. The expertise GSI has already acquired in this field ensures that the unprecedented feasibilities of the facility to come – concerning energy, intensity and experimental tools – can optimally be exploited to provide access to the fundamental facets of relativistic atomic physics and neighboring fields. The central topics will be:

- **Test of Quantum Electrodynamics (QED) in strong fields** (chapter 5.1.2.2), emphasizing the precise determination of QED contributions in the heaviest one- and few-electron atoms, in particular for the $1s_{1/2}$ and $2s_{1/2}$ states. For Li-like heavy ions, a *direct* excitation of the 2s-2p transition by Doppler-boosted, counter-propagating laser fields comes into reach at the new facility, which will tremendously improve the precision. Since the Doppler boost in the rest frame of the counter-propagating ion amounts to about 2γ (see Figure 5.2), a direct excitation of the 2s-2p transition in Li-like uranium (E = 280 eV) could be achieved at SIS200 ($\gamma = 23$) even by a frequency-doubled *visible* laser or by an x-ray laser of about 110 eV at the NESR ($\gamma_{max} \approx 1.45$). The latter option could also lead to an efficient laser cooling of fast, Li-like heavy ions.

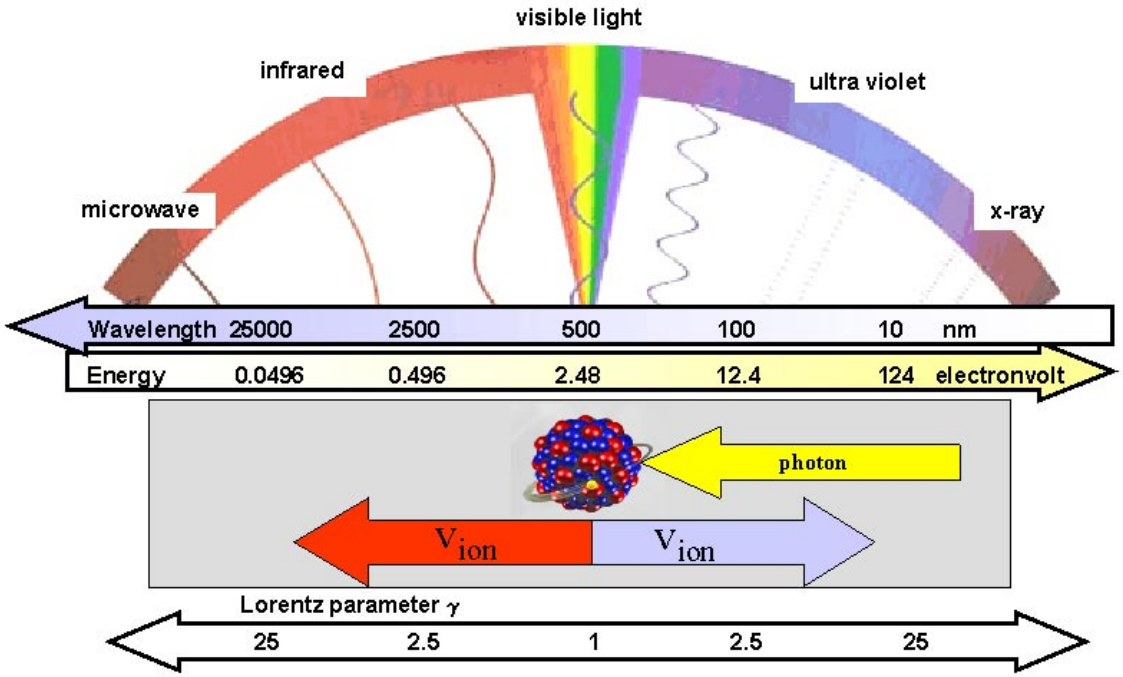

Figure 5.2: Doppler shift of a visible photon with energy $E_0 = 2.48$ eV (wavelength $\lambda_0 = 500$ nm), as seen in the ion rest frame, vs. the Lorentz factor γ. For a laser beam, counter-propagating with respect to the ion, the energy amounts to about $2\gamma E_0$ (upper part, right hand side). For a parallel laser beam the wavelength undergoes a red-shift to about $2\gamma\lambda_0$ (left hand side).

- **Application of atomic physics techniques to nuclear physics** (chapter 5.1.2.3). By means of the Super-FRS the study of nuclear charge radii and electromagnetic moments of radioactive nuclei can be addressed by collinear laser

spectroscopy in the NESR. A precise as well as highly sensitive mass determination of radioactive, highly charged nuclei becomes feasible, too, by measuring their cyclotron frequencies in the Penning trap HITRAP. For this purpose the ions are decelerated in both, the NESR and the following linear RFQ device, brought to rest and cooled finally to about 4 K in the trap.

- **Test of fundamental symmetry principles** (chapter 5.1.2.4). The unique features of the new facility together with powerful experimental tools also pave the way for highly sensitive tests of fundamental symmetry principles of physics, such as parity conservation or time-reversal invariance. Moreover, stored, cooled and polarized nuclei would allow one to search for a nuclear dipole moment, caused by a simultaneous violation of both, parity and time-reversion symmetry. By measuring beta-neutrino correlations of trapped and cooled radioactive nuclei the Standard Model of electroweak interaction can be tested with high sensitivity.

- **Ions and electrons in ultra-high intensity, femtosecond laser fields** (chapter 5.1.2.5). This novel physics including the generation of hard x rays can uniquely be investigated by the synergetic interaction of ions that are stored and cooled in the NESR, of the new laser facility PHELIX, and of the electron collider.

- **Relativistic heavy-ion beams for material research** (chapter 5.1.3). By utilizing the unique properties of relativistic heavy-ion beams for material research, hitherto unknown possibilities of three-dimensional material modification may result. The combination of high beam intensities and short ion pulses will also allow one to access the time evolution of radiation damage in condensed matter down to ultra-short time scales of 10^{-11} s.

- **Application of relativistic ions in radiobiology and space research** (chapter 5.1.4). This topic is of practical interest, because for the stopping power dE/dx only scarce experimental data exist in the true relativistic regime above 1 GeV/u. However, the underlying microscopic mechanism of energy deposition in this domain – nuclear, electronic stopping, radiative energy loss – are decisive for the effects caused by high-energetic ions of the cosmic radiation in biological tissues as well as in electronic devices. Only by using relativistic heavy-ion beams, those effects of energetic cosmic radiation in living cells and computers can be studied in a systematic way. This would allow a better risk estimation of long-term space flights (e.g. to Mars and other planets) and help to optimize shielding in a more efficient way.

The many novel possibilities at the new facility demand for different experimental areas and variable instrumentation. In SIS200 a counter-propagating laser has to be installed which utilizes the high Doppler boost for direct excitation of Li-like atoms as well as for laser cooling. The NESR, able to store and cool both stable and (long-lived) radioactive nuclei, and equipped with an internal gas jet, electron target, electron collider and with collinear laser beams, will be the workhorse for atomic physics experiments. Ion beams, extracted from the NESR, will be led either to fixed-target experiments, or they will be stopped and cooled in the HITRAP facility. Several laser

facilities including the high-power femtosecond laser PHELIX are essential parts of the instrumentation. Besides HITRAP, placed behind the NESR, additional trap facilities will be installed at the end of the Super-FRS, to probe the properties of radio-active nuclei on an unrivalled level of accuracy.

Worldwide several radioactive beam factories are planned or already under construction such as RIA (USA), MUSES (Riken, Japan) or HIRFL (Lanzhou, China). The plans at MUSES and HIRFL cover a spectrum similar to that planned for the new GSI facility. However, due to the comparatively low energies foreseen for MUSES and HIRFL, the achievable intensity of *highly-charged* heavy ions (e.g. bare uranium) should be there significantly smaller than that to be expected for the new GSI facility. Similar restrictions are valid for the existing as well as for the planned EBIT (Electron Beam Ion Trap) facilities.

5.1 Science Case

5.1.1 Introduction

For many decades, atomic physics and, in particular, atomic spectroscopy has been the basis and 'mother science' for any research addressing the structure of matter. The explanation of the discrete line spectra of the hydrogen atom was the first benchmark of quantum mechanics, the cornerstone of modern physics. Identification as well as classification of the chemical elements was first achieved by interpreting atomic spectra as their unambiguous and unchangeable fingerprints. The secular perception of the unity of the universe emerged from the analysis of the spectra of photons emitted by atoms or ions of near and distant stars, initiating a close connection between atomic physics and astrophysics that has never been interrupted. Atomic masses and nuclear ground state properties, as deduced from the interplay of atomic nuclei with their electron cloud, led to the formulation of the very first models of nuclei. Moreover, atomic theory was the first guide to the understanding of other complex systems such as molecules or crystals or even basic effects in biology and solid-state physics.

Meanwhile, quarks and leptons have replaced atoms as the most elementary building blocks of matter. Nonetheless, atomic physics is far from being a closed and 'sterile' field of physics, as demonstrated by recent breakthroughs achieved by atomic physics, such as the observation of Bose-Einstein condensation or the stupendous advances in high-precision laser spectroscopy.

Accelerator-based atomic physics has always opened new, widely unexplored fields of research. The heavy-ion storage cooler ring ESR at GSI has provided a first access to basic processes associated with strong electromagnetic fields in collisions of heavy, highly-charged ions. This has been done by various experimental methods, e.g. x-ray spectroscopy addressing the 1s Lamb shift in heavy ions, collinear laser spectroscopy of the hyperfine splitting in hydrogen-like heavy atoms, or by the investigation of dielectronic recombination in heavy, few-electron atoms. The dynamical aspect of atomic collisions has been probed by means of radiative electron capture, resonant electron transfer and first kinematically complete measurements of many-electron transitions.

The conditions of atoms mentioned above might be understood as 'extreme' with regard to our daily experience. However, the majority of matter in the universe exists as stellar plasmas, where high temperatures, high atomic charge states and high field strengths prevail. The investigation of these extreme atomic conditions is, therefore, indispensable for our understanding of the processes ongoing in the 'real' matter. The extreme field strength probed for instance by a 1s electron in a H-like heavy ion is exemplified in Figure 5.3.

Accelerators are presently the tools that are suited best to provide such extreme conditions in the laboratory. In particular the proposed new GSI facility will open up

exciting and far-reaching perspectives: it will provide the highest intensities of relativistic beams of both stable and unstable heavy nuclei, in combination with the strongest possible electromagnetic fields, allowing to extend atomic spectroscopy up to the virtual limits of atomic matter. Based on the results already achieved at the ESR, a substantial progress in atomic physics research has to be expected in this domain, due to a tremendous improvement concerning intensity, energy, and production yield of unstable nuclei.

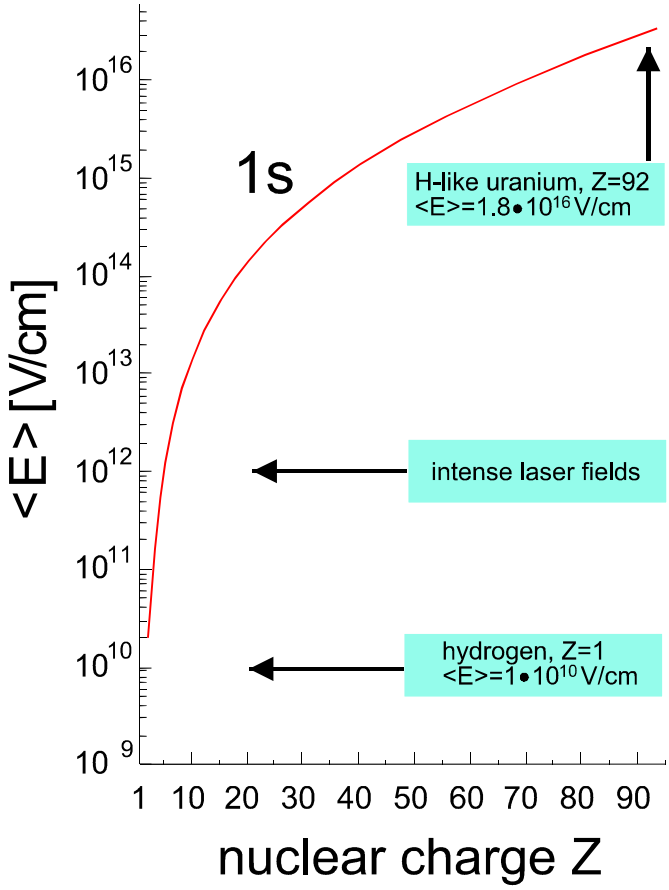

Figure 5.3: Expectation value of the electric field strength <E> for a K-shell electron in H-like ions as a function of the nuclear charge number Z. For comparison, the field active in a strong laser pulse is indicated.

Atomic physics research on relativistic, highly-charged heavy-ion beams at the new GSI facility can be associated mainly with three types of experimental studies:

- The first type uses highly relativistic heavy ions for a wide range of *collision studies* that involve photons, electrons and atoms, and exploits the large *Doppler boost* and the *rapidly varying fields* in those reactions. An understanding of those collision phenomena is required for all lines of research in atomic physics, including the interaction in solids (material research) or in living cells (radiobiology), and for accelerator technology.

- The second type uses *high-energy beams* for achieving high stages of ionization up to bare uranium nuclei. It focuses on *structure studies* for these ion species, a field being still largely unexplored, but intimately connected to *astrophysics* on the one

hand, and allowing precision tests of quantum electrodynamics in extremely strong electromagnetic fields on the other hand.

- The third type utilizes well-defined charge states of *radioactive atoms* for fundamental studies and model-independent determination of *nuclear quantities* by applying atomic physics methods. An important scenario for this class of experiments will be the slowing-down and trapping of carefully chosen nuclei in atom- or ion-traps, which will enable high-accuracy experiments in atomic and nuclear physics as well as highly-sensitive tests of the Standard Model.

Applied research in the field of relativistic heavy ions is primarily based on the understanding of the elementary atomic collision processes. The interaction of those ions with material together with the involved secondary processes determines alterations in bulk material and in living cells. The long ranges of relativistic ions allow to penetrate deeply into large devices and the high Z of heavy ions leads to especially large interaction cross sections. Hence, fundamental research in theses fields will be a necessity for space research, material tests and radiobiology.

5.1.2 Atomic Physics Research

5.1.2.1 Relativistic Collision Dynamics in Strong Electromagnetic Fields

The study of the dynamics of highly relativistic ion-atom collisions extends the frontiers of our present knowledge about the interaction of charged particles with extremely strong, rapidly varying electromagnetic fields. The *transverse* electric and magnetic components of the electromagnetic fields associated with the moving ions steadily *increase* with γ and become almost equal in magnitude while the duration of the electromagnetic pulse decreases (see Figure 5.4). This is clearly a relativistic effect. In the relativistic domain, cross sections and impact parameter dependences of elementary processes such as ionization, excitation, electron capture and pair production (see Figure 5.5) are dramatically affected by the strong dependence on the velocity of the transverse electromagnetic field of the projectile. As an illustrative example, Figure 5.6 shows the energy dependence of an electronic transition in a high-Z projectile as produced by Coulomb excitation. The displayed ln(γ) increase of the cross section holds true for all other kinds of excitation-like processes such as ionization and e^+-e^- pair creation. A precise understanding of the relativistic quantum dynamics offers the key for the advance of our basic knowledge in the physics of strong fields.

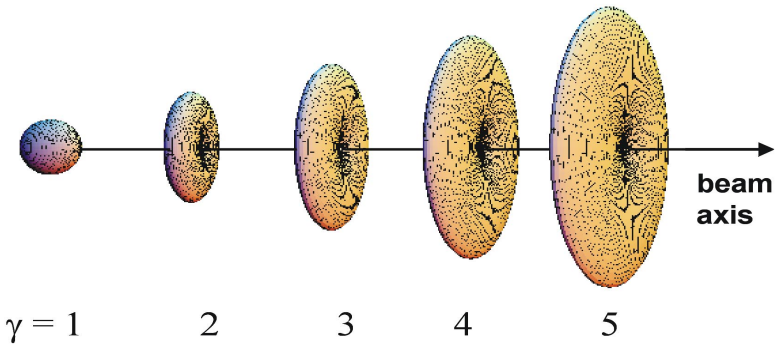

Figure 5.4: Dependence of the electric radial field strengths for a point charge on the Lorentz factor γ (γ = 1,2,3,4 and 5 corresponds to 0, 87, 94, 97, and 98 % of the speed of light).

Ion-Atom Collisions

Utilizing the high luminosity of the planned new GSI facility, differential aspects of atomic processes at high energies that are beyond inclusive cross section studies become accessible, for which the electromagnetic interaction differs significantly from the low-energy regime [1]. For example, a measurement of the impact parameter dependence for both inner-shell ionization and excitation processes will enable the separation of the longitudinal and the transversal field contributions to the interaction. For such investigations the spectroscopy of photons as well as electrons and positrons is required. The photon emission gives the details of the specific excitation mechanism in those fields. It also offers the special opportunity to study angular resolved photoionization at very high energies by means of its time reversed

process, the radiative electron capture (REC) [2]. One may mention the search for recombination followed by e^+-e^- pair production instead of photon emission. This higher-order process, presumably requiring high collision energies, is similar to di-electronic recombination, but with the electron being excited from the negative to the positive continuum.

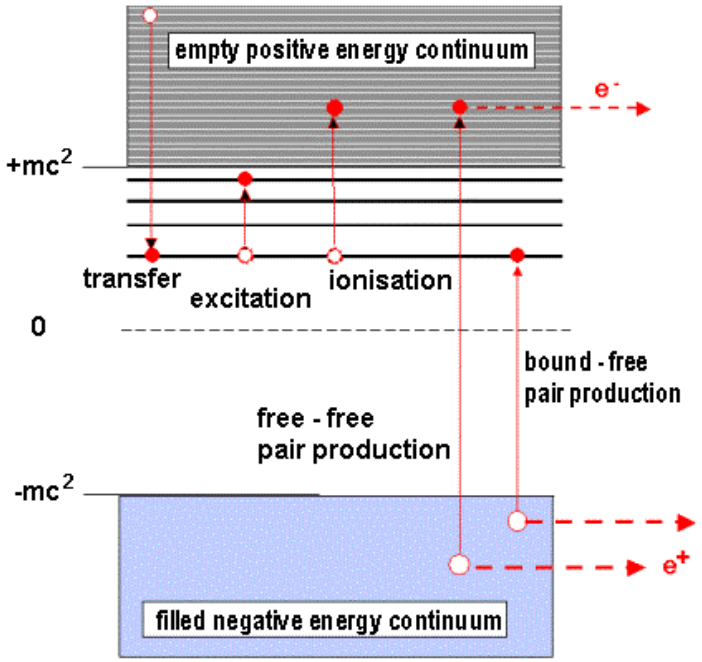

Figure 5.5: Energy diagram of the single-particle Dirac equation and basic atomic processes which occur in ion-atom collisions.

The momentum transfer associated with the virtual photon field is small enough that the correlated initial momenta of the bound leptons remain nearly unperturbed. While the field strengths produced in such collisions are orders of magnitude larger than those associated with other excitation techniques (e.g. synchrotron radiation, strong laser pulses, plasma pinch devices etc.), the duration of the interaction is much shorter (10^{-22} s < t < 10^{-18} s). One goal of future experiments will be the measurement of the complete momentum balance in relativistic collisions both in transverse and in longitudinal direction by detecting the emitted electrons/positrons in coincidence with the recoiling target ion [3]. From measuring the momenta of the electrons/positrons and the recoil ion with high relative accuracy, direct information on the correlated many-lepton dynamics can be obtained. Also, high-resolution electron spectroscopy will allow a unique isolation of the relativistic and quantum-electrodynamical contributions to the electron-electron interaction in strong fields.

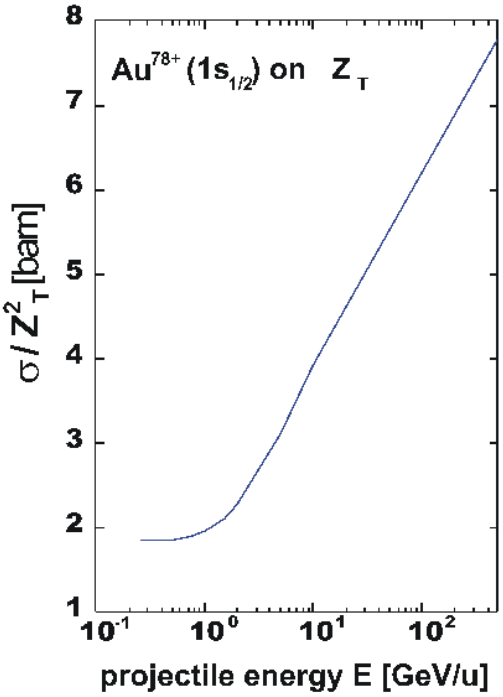

Figure 5.6: Reduced excitation cross section σ / Z_T^2 associated with the $1s_{1/2} \rightarrow 2p_{3/2}$ transition in hydrogen-like gold ions colliding with a light target atom Z_T as function of the projectile energy E [4].

The new facility with an option for merged or crossed beams would provide sufficient intensity to study electron binding energies in critical and supercritical electromagnetic fields using quasi-molecular interference effects. The merged or crossed beam option would be a break-through for the spectroscopy of the 1sσ-orbital of super heavy quasi-molecules. Thus the very fundamental problem of the behavior of bound electrons in supercritical fields can be addressed in an unequivocal manner, i.e. answering whether the 1sσ-level becomes a resonance in the negative energy continuum [5]. In the experiments on pair production performed so far at GSI this process was suppressed by Pauli blocking. Pair production in high-Z systems is particularly interesting for close collisions at *low (relative) energies* where one expects the formation of atomic quasimolecules. This results in the tenfold increase in binding energy of the 1s state and leads to enhanced positron production since the 1s state approaches or even (in supercritical collisions) enters the antiparticle continuum of the Dirac equation (Figure 5.7).

Electron capture into the 1sσ and 2pσ states will become the dominant mechanism for pair production, leading to an enhancement of up to two orders of magnitude compared to collisions of ions which are not fully stripped. The large collisional broadening precludes a direct spectroscopy of superheavy quasimolecules and the identification of spontaneously produced positrons ("decay of the vacuum") [5]. However, by precisely measuring the bound-free pair production rates and their dependence on nuclear charge, energy, impact parameter and final state distributions it will be possible to draw conclusions on the quasimolecular energies in an indirect way. Pair production is very sensitive to the strong binding and an agreement between theory and experiment would confirm the validity of QED of strong fields in a quantitative way.

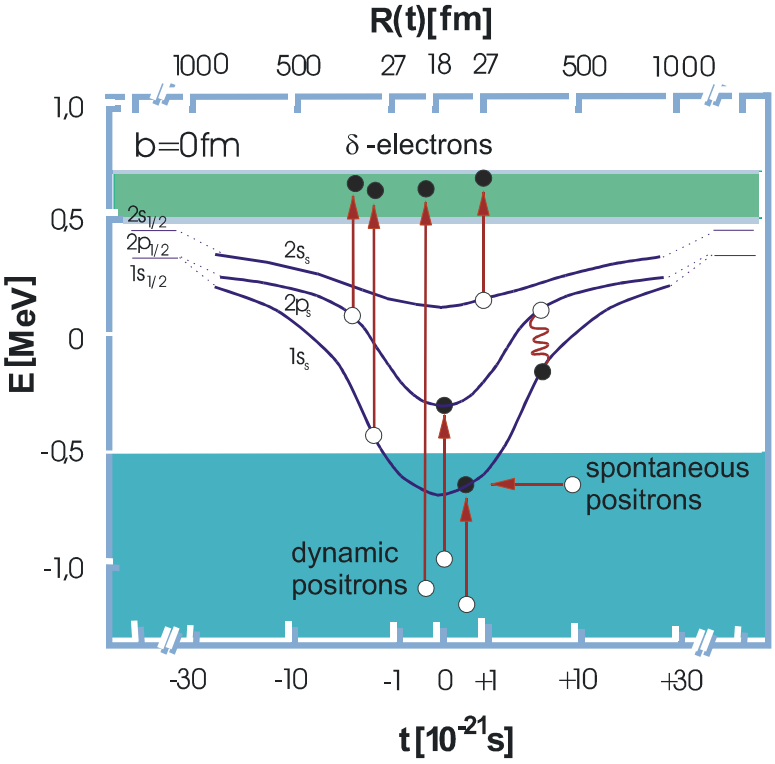

Figure 5.7: Electron-positron pair creation into the quasimolecular 1sσ level in a collision of bare uranium ions. The binding energies of the states are plotted as function of the collision time. Deviations from the binding energy predicted by QED would be visible in the pair production rate.

Electron-Positron Pair Production at Relativistic Energies

As a result of the large electromagnetic fields associated with heavy ions in *relativistic* motion, pair production becomes a very important reaction channel. For asymptotically high energies ($\ln \gamma >> 1$) and in the lowest order of perturbation theory, the cross section for *free pairs* is written as [6]

(5.1)
$$\sigma^{\text{free–free}} \propto Z_T^{\,2} \cdot Z_P^{\,2} \cdot \ln^3(\gamma/4)$$

where Z_P and Z_T are the charge numbers of projectile and target, respectively. The dependence of the cross section on collision energy and nuclear charge in Eq. (5.1) clearly shows that for encounters involving highly-charged heavy ions in relativistic motion the production of pairs is dramatically enhanced, making this process specific to relativistic atomic collisions. In addition, the special case of pair production with the electron created in a bound state of one of the colliding ions – the so called *bound-free pair production* (see Figure 5.5) – changes the charge state of that ion and is one of the main loss processes for ions in relativistic heavy-ion colliders. Bound-free pair creation was recently used at CERN and Fermilab for the production of anti-hydrogen $\overline{H} = (\bar{p}e^+)$, the simplest anti-atom that consists of an antiproton ($\bar{p}$) and a positron

(e^+). The parametric dependence of the asymptotic high-energy cross section is given in perturbation theory [7] by

(5.2) $$\sigma^{\text{bound}-\text{free}} \propto Z_T^{\,2} \cdot Z_P^{\,5} \cdot \ln(\gamma/\Delta),$$

where Δ is a slowly varying parameter depending on Z_P, the charge number of the ion capturing the electron. Explicit calculations [8] yield values close to 10 barn for a uranium on uranium collision at 10 GeV/u ($\gamma \approx 10$).

Whereas the above given expressions are expected to be valid only for extreme relativistic collisions, a non-perturbative treatment is compulsory for the collision energies covered by the new GSI facility ($2 \leq \gamma \leq 23$). Note that at extreme energies, in the region of hundreds of GeV/u, there is good agreement between theory and experiment [9]. However, the situation is much less satisfactory at intermediate relativistic energies of a few GeV/u. Here, even the target charge dependence is not well understood [10]. There are very few and only inclusive measurements of pair production available in the intermediate relativistic regime, the new facility would be the only one capable worldwide of filling this important gap. In particular, differential measurements as function of the impact parameter are urgently needed since they are expected to display the non-perturbative dynamical structure of the QED vacuum. This is especially true for bound-free pair creation where at small impact parameters the strong electromagnetic field can lead to an enhanced production probability.

All these processes can be studied at an experimental area behind the SIS 200 in single-pass and fixed-target experiments at γ-values up to $\gamma \approx 20$. Of particular interest is the unique potential provided by the high-energy storage ring (HESR) for precise reaction studies. Here, the collisions of intense and cooled relativistic ion beams ($\gamma \approx 6$) with low-density gaseous matter, provided by the internal gas-jet target can be studied under unprecedented clean single collision conditions.

5.1.2.2 Test of Quantum Electrodynamics in Strong Fields

X-Ray Spectroscopy

Quantum electrodynamics (QED), the basis and cornerstone of all present field theories, is still the best confirmed theory in physics. Yet, despite the enormous success of QED in predicting the properties of electrons in weak fields, a precise test in the strong-field limit where novel phenomena might show up, is still pending. Thus, a primary goal is to explore the behavior of electrons in the strongest electromagnetic fields accessible to experimental investigation. Precision measurements of electron binding energies are best suited to deduce characteristic QED phenomena in intense fields. Therefore, the comparison of predicted with experimentally determined level energies of strongly bound electrons provides a critical test of QED in strong fields.

The proposed heavy ion accelerator combined with novel experimental techniques such as excitation by laser light or channeling in crystals will provide a unique tool to determine comprehensively for example the 1s binding energy in the heaviest one-electron ions with the highest possible accuracy. This is also true for the exploration of the fundamental electron-electron interaction in the strong field limit by combined laser, x-ray and electron spectroscopy.

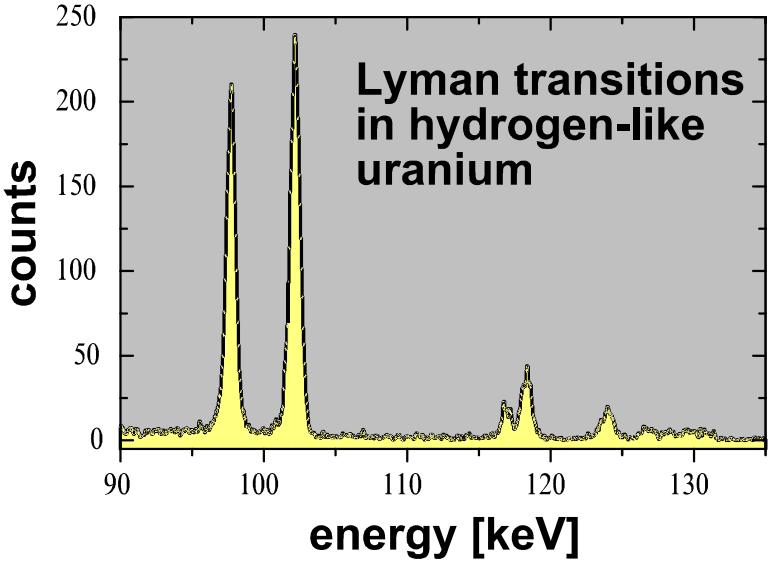

Figure 5.8: X-ray spectrum measured at the ESR/GSI associated with Lyman transitions in hydrogen-like uranium [11]. The Lyman-α lines are near 100 keV, the Lyman-β lines near 118 keV, etc.

For the case of hydrogen-like uranium, where the ground-state binding energy amounts to 132 keV, the 1s Lambshift has been determined with an accuracy of 13 eV based on the x-ray spectrum shown in Figure 5.8. A measurement of the 1s Lamb shift (465.8 eV) with an accuracy of 1 eV and below still remains one of the most important tests of QED in strong fields [12]. In addition, the development and understanding of bound-state QED in strong fields can be improved significantly for many-body systems by measuring, e.g., the $2s_{1/2}$ - $2p_{1/2}$ splitting in Li-like uranium (≈

280 eV) to an accuracy of 10^{-2} eV. Heavy lithium-like ions are particularly well suited because the electron-electron interaction contributions can be calculated reliably and the relatively low atomic excitation energies are strongly influenced by QED effects. Figure 5.9 shows the level scheme of lithium-like uranium with the $2s \rightarrow 2p$ transitions. To achieve the required high spectroscopic accuracy, laser based techniques appear to be most promising.

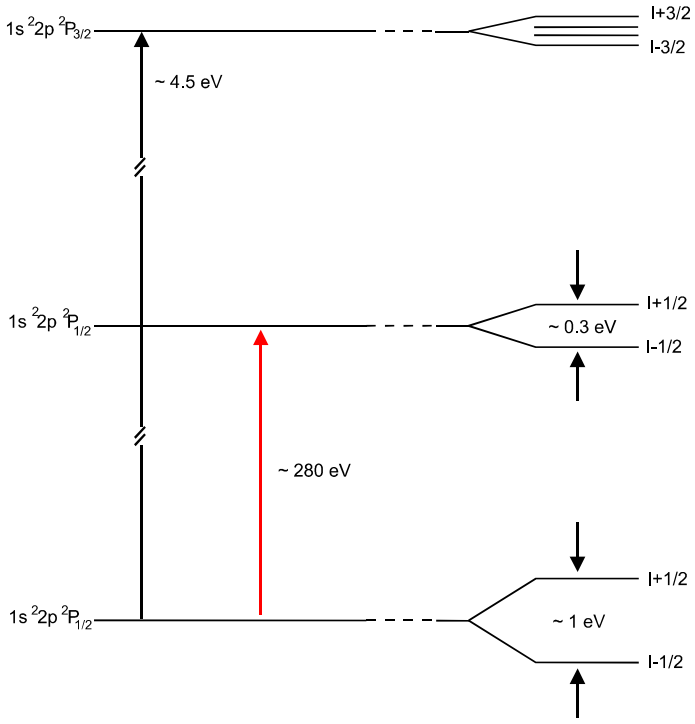

Figure 5.9: Level diagram of lithium-like uranium. The 2s1/2 to 2p1/2 transition energy of 280 eV is within the range of laser-pumped X-ray lasers at the NESR or of conventional lasers in the optical regime at SIS 200 via the Doppler boost. The HFS splitting for an isotope with nuclear spin is indicated on the right side.

Laser Spectroscopy

A typical application of precision laser spectroscopy will be the excitation of transitions starting from the ground state of highly charged, e.g. lithium-like ions. At the NESR, photon energies of around 110 eV in the laboratory frame would be sufficient to induce the 280 eV $2s_{1/2}$ - $2p_{1/2}$ transition in uranium when the laser light is counter-propagating to the ions. Such a source could be provided by an X-ray laser pumped by multi-terawatt pulses from the 10 J front-end of the laser system PHELIX presently under construction at GSI [13]. The experimental procedure will be similar to the established scheme used for laser spectroscopy of the ground-state hyperfine splitting in hydrogen-like ions. Light emitted after laser excitation is detected in the forward direction. This leads to an additional Doppler shift into an energy range between two and three times the laser energy. These energetic photons can be efficiently and selectively detected. Another application will be the study of low-lying metastable states in moderately charged heavy ions. In these cases many-electron correlation effects can be studied in great detail.

Alternatively, exploiting the higher energies available in the SIS200, even photon energies in the visible range will be sufficient for excitation of the $2s_{1/2} - 2p_{1/2}$ transition in lithium-like uranium. For such ions, a beam energy of 21.3 GeV/u corresponding to a Lorentz factor of $\gamma = 23.9$ can be reached at SIS200. Since after laser excitation the emitted photon again will be strongly Doppler shifted, high detection sensitivity and good suppression of scattered laser light can be reached. Also, fixed-frequency lasers can be used because they can be tuned via the Doppler shift. The proposed experimental setup is shown in Figure 5.10.

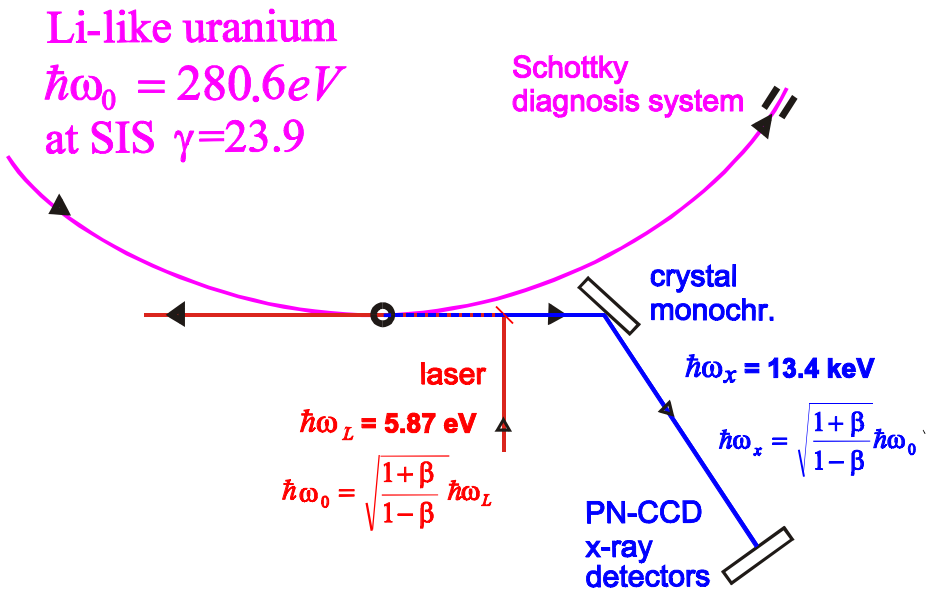

Figure 5.10: Experimental setup for precision transition-energy and hyperfine-structure measurements in lithium-like systems at the SIS200 ring.

The experimental setup consists of the combination of two very precise experimental methods which are based on a laser and a x-ray crystal spectrometer. The $2s_{1/2} - 2p_{1/2}$ transition can be excited for all elements up to uranium with a pulsed frequency-doubled laser beam. For the case of lithium-like uranium, a laser photon energy $\hbar\omega_L = 5.87$ eV is shifted in the moving system to $\hbar\omega_0 = 280.6$ eV which is the $2s_{1/2} - 2p_{1/2}$ transition energy. The emitted fluorescence photon is boosted into the hard x-ray region and appears in the laboratory system in the forward direction at $\hbar\omega_x = 13.4$ keV. If the x-ray energy is measured with the x-ray crystal spectrometer both, the transition energy and the Lorentz factor γ can be calculated according to the equations

(5.3)

$$\hbar\omega_0 = \sqrt{\hbar\omega_L \cdot \hbar\omega_x}\,, \qquad \gamma = \frac{1}{2}\sqrt{\frac{\hbar\omega_x}{\hbar\omega_L}}\,.$$

It has been pointed out [14] that with currently existing laser systems with a relative line width of 5×10^{-7} and a mean power of 5 W at a repetition rate of 10 kHz, shining on a collection of 10^6 lithium-like ions circulating as a bunch with an energy spread of 10^{-4} and observed by an x-ray monochromator with a resolution of 5.7×10^{-5}, the transition energy of 280 eV in uranium can be measured with an accuracy of 0.007 eV within one hour. Compared with the currently best value of 280.59 ± 0.09 eV [15], this will lead to an increase in precision by a factor of 10 and will provide a highly sensitive test of QED and relativistic-correlation calculations for three-electron systems.

Highly-Charged Ions in Traps

Along with the precision measurements of binding energies (Lamb shift), measurements of the g factor of the bound electron in highly-charged ions provide a sensitive test of bound-state QED calculations in strong electromagnetic fields.

The ratio of the g factors of the bound electron in hydrogen-like ions to that of the free electron as a function of Z is given by

(5.4)
$$g_{bound} / g_{free} = 1 - (\alpha Z)^2 \cdot \left(\frac{1}{3} - \frac{\alpha}{4\pi} \right)$$

where the 1/3 term originates from the relativistic Dirac equation and $\alpha/4\pi$ is the first-order QED correction. Figure 5.11 shows the dependence of the Dirac and bound-state QED corrections to g_{free} as function of the nuclear charge [16,17]. The QED corrections contribute in U^{91+} on the level of 10^{-3}. Nuclear size corrections are of the same order but can be calculated to an accuracy of 10^{-4} so that the theoretical uncertainty of the bound g factor in U^{91+} is of the order of 10^{-7}. If in addition the g factor of the electron in the 2s-state of the lithium-like ion is measured, it can be expected that as in the case of the 1s hyperfine structure [18], the uncertainty of the nuclear size correction drops out and the full experimental accuracy of ppb can be exploited for the QED test.

For the determination of the g factor of the bound electron in highly charged ions, a precision Penning trap was developed at GSI and the University of Mainz. A recent experiment on hydrogen-like carbon $^{12}C^{5+}$ [19] yielded an accuracy of a few ppb, $g_e^{exp}(C^{5+})$ = 2.001 041 596(5) for the g-factor of the bound electron. This result is in excellent agreement with the theoretical value of $g_e^{th}(C^{5+})$ = 2.001 041 591(7). This is one of the most stringent tests of bound-state QED.

In order to extend the g factor measurements to hydrogen-like uranium U^{91+}, a trap facility for capturing and cooling of highly-charged ions produced at the future GSI-accelerator complex is planned. Hydrogen-like heavy ions will be accumulated, cooled and decelerated in the NESR to 3 MeV/u. After ejection from the NESR they will be further decelerated in a linear decelerator structure to be captured in a cryogenic Penning trap operated as a cooler. After cooling to 4 K, the ions are transferred to the

precision Penning trap for g-factor measurements. A pilot facility will be the Heavy-Ion TRAP (HITRAP) facility to be installed at the present Experimental Storage Ring ESR [20].

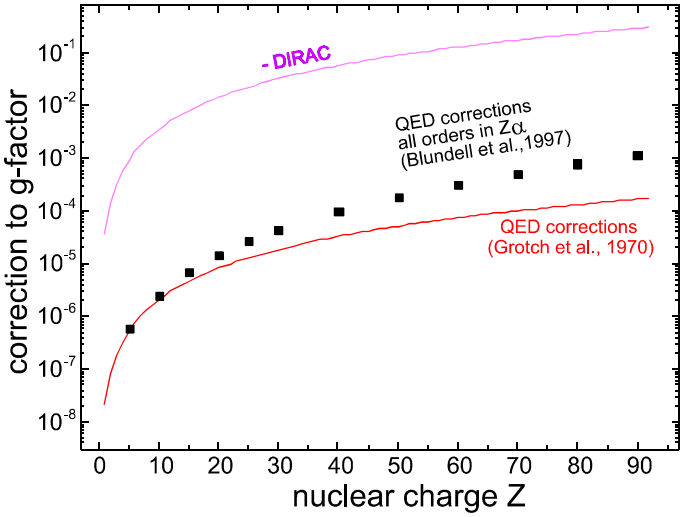

Figure 5.11: Bound-state corrections to the g factor of the electron in hydrogen-like ions as function of the nuclear charge.

Electron-Ion Recombination

Dielectronic recombination (DR) of ions, having at least one electron, with free electrons turned out to be a novel and sensitive tool for precise structure studies. The possibility of producing highly-charged heavy ions and of storing them as low-emittance ion beams in a storage ring opened a new window for the investigation of the recombination of ions and electrons at low relative velocities. In this resonant process a free electron is captured and the excess energy excites one of the bound electrons to a higher state. This is the time-reversed Auger effect. The initial interest in these processes arose from the need to understand astrophysical and fusion plasmas.

The potential of recombination experiments for spectroscopy has been already demonstrated at the ESR. In these experiments, the ESR electron cooler served as a tunable electron target. The electron energy was switched repeatedly for short periods, typically 25 msec, between the cooling energy and the energy of interest, and the recombination rates were recorded as a function of the relative energy between the electrons and the ions. Figure 5.12 shows the spectrum measured for lithium-like gold together with fully relativistic theoretical calculations. It is worth emphasizing that no parameter has been fitted to the data. The theoretical curve has been only folded with the electron temperature to yield an energy resolution of ≈ 0.7 eV. The DR measurements provide information on both electron-electron interactions in the presence of a strong central field and on the ionic structure of the investigated species. Additionally, a novel experimental method to extract the $2s_{1/2}$ - $2p_{1/2}$ splitting by measuring DR-resonances associated with capture of a free electron into very high Rydberg states (n > 20) has been developed. An extrapolation of the measured

resonance energies up to n = ∞ leads to the sought value sensitive to the Lamb shift of the 2s level. The precision and significance is enhanced by the statistical redundancy. It is planned to extend this method to hydrogen-like heavy ions, where additional interference effects between radiative (RR) and dielectronic recombination as well as of neighboring resonances can be studied.

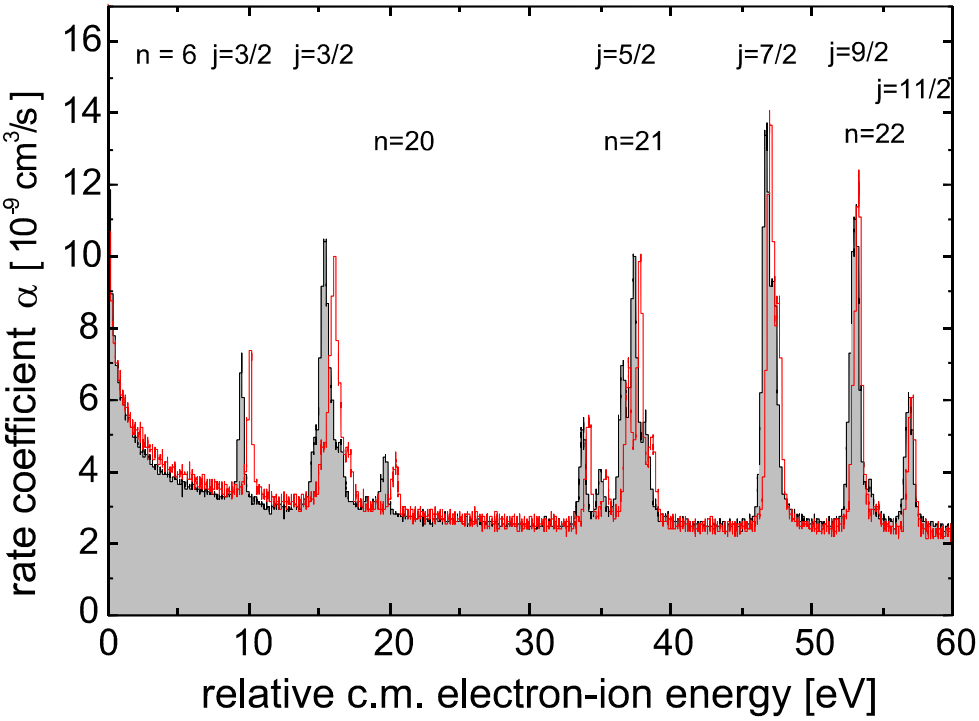

Figure 5.12: Experimental data (gray shaded area) [21] and theoretical predictions (dotted line) [22] folded with the electron temperature for the dielectronic recombination of lithium-like gold (e^- + Au^{76+} ($1s^2 2s$) → Au^{75+} ($1s^2 2p_{1/2} nl_j$) or ($1s^2 2p_{3/2} 6l_j$)). On an absolute scale, the theoretical energies deviate from the experimental ones by 0.4 eV on the average.

The NESR with a second independent electron target will allow for the first time the study of the electron-electron interaction also for the innermost bound electrons in very heavy systems. At the ESR, having no second electron target, such studies were not possible up to now. An independent electron target at the NESR will allow also to improve the precision and accuracy of the measurements since the ion beam can be cooled permanently during the DR experiments.

5.1.2.3 Atomic Physics Techniques Applied to Nuclear Physics

The very first precise information on properties of nuclei came from atomic spectroscopy and mass spectrometry. By these methods the interaction of the nucleus with the electromagnetic field produced by the electrons surrounding the nucleus, or with an externally applied electromagnetic field, was investigated. In this way, the nuclear ground state spins, moments, charge radii, and masses of stable nuclei and of many radioactive nuclei [23] have been determined (Figure 5.13). It should be noted that the optical techniques, based on hyperfine structure splitting (HFS) or isotope shift measurements, yield *model-independent* information about the nucleus [24]. However, the hyperfine fields produced by the many electrons of a neutral atom at the site of the nucleus can only be calculated with an accuracy of at best 1 % in favorable cases such as the alkali elements. An exception in this context is a newly proposed and possibly far-reaching method [25], namely to address the g-factor of low-lying rotational nuclear states by measuring the hyperfine-quenched atomic lifetimes of highly-charged ions.

In the case of isotope shifts and deduced changes in charge radii, the accuracy of the calculation of the electron density at the site of the nucleus is usually not better than 10 %. The same holds true for magnetic HFS and the extracted nuclear magnetic moments where the magnetic field produced by the electrons at the site of the nucleus has to be calculated. Up to 30 % uncertainty results in the case of electric field gradients required to extract nuclear electric quadrupole moments from the electric HFS. Here, one or few-electron systems, as provided at GSI, have the advantage that the hyperfine fields can be calculated with high accuracy.

Nuclear Spins, Moments and Charge Radii

On-line laser spectroscopy in combination with powerful isotope production and separation facilities allow one to study the nuclear properties of ground and isomeric states of short-lived, exotic isotopes which are only available in small quantities [26]. Since the model-independent data are collected in long isotopic chains reaching far

from the valley of nuclear stability, these data provide clear information on single-particle as well as collective nuclear effects and enable stringent tests of nuclear models. Furthermore, new phenomena might be discovered which do not show up in stable or long-lived isotopes or which can only be detected as deviation from systematic trends of neighboring isotopes. A striking example is the nuclear shape coexistence and shape transition detected by optical spectroscopy in the mercury region.

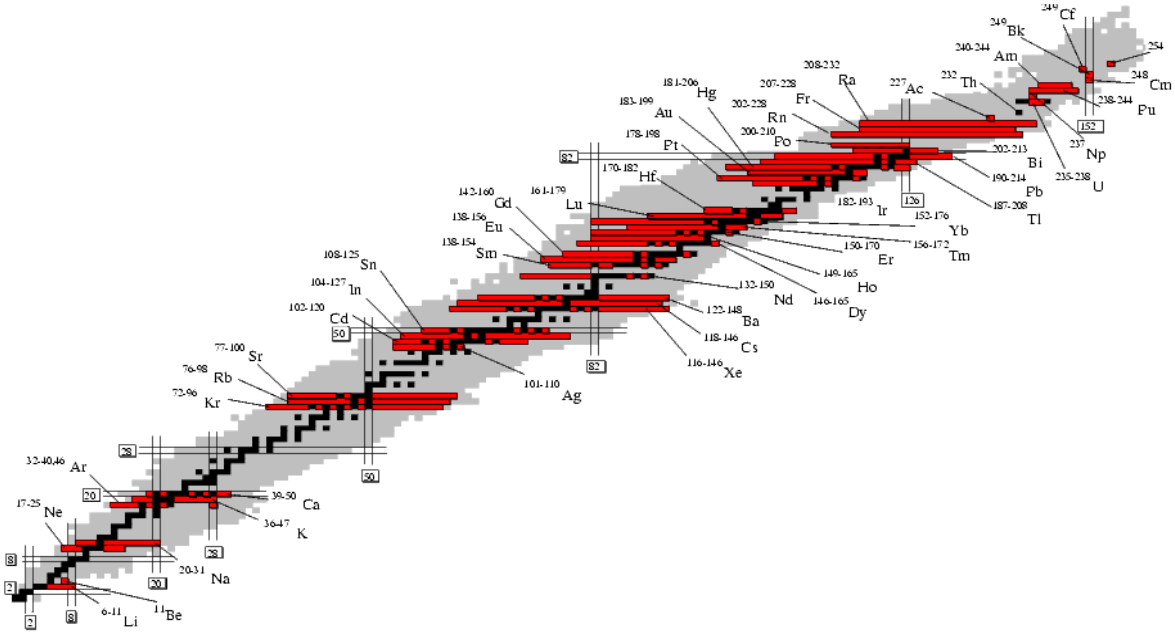

Figure 5.13: Chart of nuclei showing the isotopes for which optical spectroscopy has been performed in long isotopic chains and on nuclei far from stability.

Today, mainly two laser techniques are applied: Resonance Ionization Spectroscopy (RIS) of neutral atoms and Collinear Laser Spectroscopy (CLS) of neutral atoms and of singly- and highly-charged ions. In general, the first technique offers the highest sensitivity while the second provides the highest resolution. The present limit for the minimum yield for collinear laser spectroscopy is of the order of 100 ions/s and the shortest-lived isotope investigated is ^{11}Li with a nuclear half-life of $T_{1/2}$ = 9 ms. By resonance ionization spectroscopy, the HFS and the IS of radioactive atoms with a nuclear half-life as short as $T_{1/2}$ = 1 ms (^{244f}Am) has been determined at a production rate of about 10 ion/s. In principle, isotopes with shorter ground-state half-lives would still be accessible by laser spectroscopy, which depends only on the production yield and not on the nuclear half-life.

Up to now, most of the optical investigations on short-lived isotopes were performed at ISOL facilities where the radioactive products have to diffuse out of the target matrix. Therefore, no or little information is available for nuclides with half-lives of less than 100 ms or for isotopes of elements which do not diffuse out of the target material because they are non-volatile or chemically reactive. Here, the universal, fast and chemically non-selective production technique of projectile fragmentation and fission as applied at GSI as well as the increased yields available at the planned new facility, will enable extension of the knowledge of nuclear ground state properties in isotopic chains to regions further away from the valley of nuclear stability.

Facility	Method	Charge State	Detec-tion	Mea-sured	Minimum No. of Particles	Minim. $T_{1/2}$	Reso-lution	Remarks
SIS200	CLS	Li-like	x-rays	HFS, IS	10 stored	1s	medium	re-injection from NESR
NESR	CLS	Li-like	x-rays	HFS, IS	10^5 stored	100 ms	low	x-ray laser/PHELIX
NESR	CLS	H/ Li-like	photons	HFS	10^6 stored	100 ms	high	M1-transition
HITRAP	FS	H/ Li-like	photons	HFS	10^3 stored	10 s	high	M1-transition; cooled to 4 K
gas cell	RIS	neutral	ions	HFS, IS	1/s	1 ms	low	directly in gas cell
gas cell	FS	1+	photons	HFS, IS	10^4 stored	10 ms	high	ion trap at room temperature
gas cell	CLS	neutral/ 1+	various	HFS, IS	10^2/s	10 ms	high	cooled to room temperature
gas cell	RIS	neutral	ions	HFS, IS	10^4/s	10 ms	medium	after re-acceleration
NAT	FS	neutral	photons	HFS, IS	1 stored	10 ms	high	restricted to some elements

Table 5.1: Different laser spectroscopic schemes for radioactive nuclides at the planned GSI facilities. CLS: collinear laser spectroscopy; FS: fluorescence spectroscopy; RIS: resonance ionization spectroscopy; HFS: hyperfine structure; IS: isotope shift; R: resolving power; NAT: neutral atom trap; 1+: singly-charged ions.

There are quite a number of different, interesting scenarios for laser spectroscopy at the new GSI accelerator facilities which are rather complementary. As shown by the overview given in Table 5.1, there is no general, ideal technique for all isotopes of all elements which are available as radioactive ion beams. In addition, until now only collinear spectroscopy of H-like systems in a storage ring and resonance ionization spectroscopy in a gas cell have been tested under experimental conditions such as at the future GSI facility. Finally, the transfer efficiencies (not given in Table 5.2) into the measuring devices are quite different for the different schemes. Laser spectroscopy to probe nuclear properties of atomic nuclei will be feasible at the new facilities at the following stations:

SIS200: A quite universal, sensitive method for precision measurements at intermediate resolving power is obtained by accumulation and cooling of the nuclei produced in the NESR storage ring, re-injection as lithium-like systems into the SIS200, and acceleration to the maximum possible energy of close to 22 GeV/u (see Figure 5.10) and discussion in Chapter 5.1.2.2). Besides the isotope shift in the 2s-2p transition, the magnetic hyperfine splitting of the $2s_{1/2}$ and the $2p_{1/2}$ states can be obtained with two laser beams the frequencies of which are de-tuned just according to the splitting of the $2s_{1/2}$ ground state (see Figure 5.9). A quadrupole splitting can only be measured if the $2p_{3/2}$ state is accessible which is the case for elements with $Z < 45$ [27]. Such experiments are possible with as few as 10 stored ions. To obtain the

magnetic dipole or the electric quadrupole moments from these measurements the nuclear spin has to be determined separately.

NESR: The magnetic hyperfine splitting in the ground state of hydrogen- or lithium-like ions can be measured by inducing M1-transitions between the hyperfine levels of the ground state as demonstrated at the ESR for $^{207}Pb^{81+}$ [28] and $^{209}Bi^{82+}$[29]. Here, the sensitivity is restricted due to the low M1-transition rate and the applicability is limited to heavier nuclides where the hyperfine splitting matches available laser wavelengths. With an x-ray laser, pumped by the ps-pulse of the PHELIX laser, the strong E1-transition from the 2s to the 2p-state can be induced. Presently, the repetition rate of PHELIX, 1 pulse/min, is rather low resulting in a reduced sensitivity. In the future, a laser with a higher repetition rate is needed which will not be a basic problem due to the rapid progress in laser technology.

HITRAP: The Heavy Ion TRAP facility HITRAP installed behind the NESR will allow for similar experiments as discussed above for the case of laser spectroscopy in the NESR but with ions nearly at rest in space and cooled to 4 K. Due to the time required for the deceleration and cooling process, the nuclei should have a half-life longer than about 10 s. However, the nearly complete elimination of the Doppler effect and the localization of the stored ions will result in extreme accuracy and sensitivity. The measurement of the Zeeman splitting of the hyperfine structure in the ground state of hydrogen-like ions will yield the nuclear g-factor. In combination with the measured nuclear g-factor, measurements of the hyperfine splitting in hydrogen-like ions will give information about the distribution of the nuclear magnetization within the nucleus. The comparison of nuclear g-factors in hydrogen-like ions with the nuclear g-factors in neutral atoms will for the first time facilitate tests of the calculations of the diamagnetic shielding correction.

Gas cell behind Super-FRS: A gas cell used to stop high-energy radioactive beams delivered by the super fragment separator (Super-FRS) will enable different kinds of laser spectroscopic experiments. One possibility is resonance ionization spectroscopy on the resulting neutral species in the cell itself. The technique has been recently successfully demonstrated for the case of isotope shift measurements of superdeformed isomeric states in Am isotopes [30]. High sensitivity as well as a low half-life limit is obtained on the expense of resolution. Another possibility is to transfer the ionic species from the gas cell to an ion trap or to produce, after cooling in a gas-filled segmented Paul trap, a low-emittance ion beam with an energy of several 10 keV. Here, collinear laser spectroscopy, resonance ionization spectroscopy, or other optical techniques can be applied [26].

Neutral atom trap: A neutral atom trap installed behind the gas cell can be used to perform laser spectroscopy with very high resolving power [31] and isotopic selectivity [32]. Presently, the technique is restricted mainly to noble gases and alkalis. Quite a number of atomic transition wavelengths, atomic life-times, HFS and hyperfine anomalies have been determined recently for francium isotopes [31]. Although single-atom sensitivity is reached [32], the efficiency for loading neutral atom traps has to be

increased. This is one of the results expected from the European RTD network NIPNET. In this way more rare isotopes produced in the new GSI facility could be studied.

Dielectronic Recombination, a Tool to Determine Nuclear Charge Radii

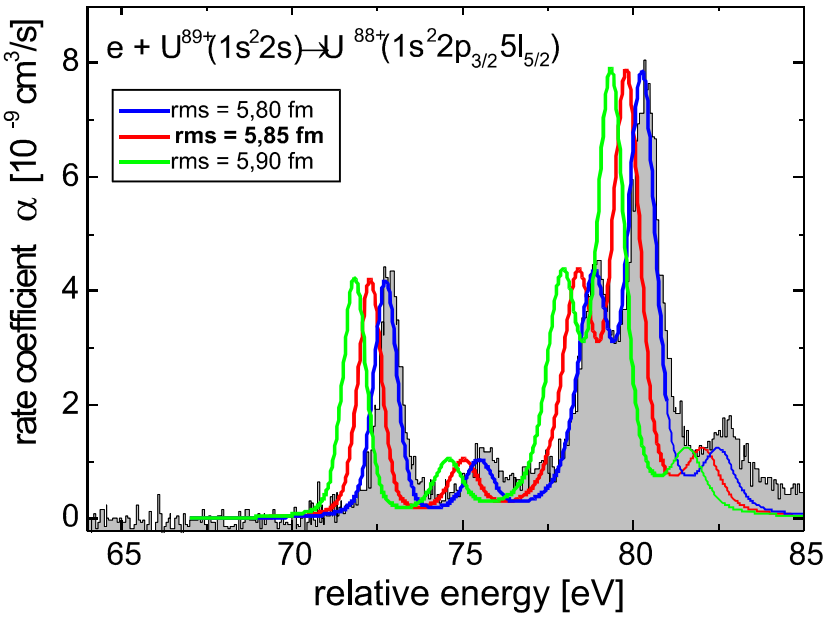

Figure 5.14: Experimental data (gray-shaded area) [33] and theoretical calculations for three different rms radii of 238U [34] for the 2p3/2 n=5 j=5/2 resonance group in lithium-like uranium.

Dielectronic recombination (DR, see Chapter 5.1.2.2) also allows studies of nuclear charge radii. This method is applicable to radioactive isotopes with a half-life longer than about 1 min. If the free electron is captured into a low-lying bound state, the comparison of precise measurements with theory can be used as a novel tool to determine nuclear radii. As an example Figure 5.14 shows measured rate coefficients α (shaded area) together with results of calculations (solid lines) for a resonance group in lithium-like uranium associated with capture of a free electron into the n = 5 shell and a $2s_{1/2}$ - $2p_{3/2}$ excitation. The line shape reflects the natural line-width as the experimental resolution is better than 0.7 eV. As can be seen, small changes of the nuclear radius lead to measurable energy shifts. Still the potential of this novel technique has to be explored experimentally as well as theoretically. Obviously, the accuracy of the measurements can be enhanced considerably by use of an electron target in the NESR and by investigating differences of charge radii along isotopic chains.

Precise Mass Measurements

For a general exploration of the nuclear mass surface in the chart of nuclei an accuracy in the mass determination of $\Delta m/m = 10^{-6}$ - 10^{-7}, as planned by TOF or Schottky mass spectrometry in the CR and NESR, respectively, is in general sufficient. However, these techniques rely on accurately known reference masses. Those can be supplied by Penning mass spectrometry in a trap behind the gas cell very similar to SHIPTRAP [35] or ISOLTRAP [36]. Here, mass measurements can be

performed on singly-charged ions with an accuracy of $\Delta m/m = 10^{-8}$ for isotopes with a half-life of 1 s or longer and with 10^{-7} accuracy for isotopes with half-lives of 100 ms.

In some cases such as double-β-decay or weak interaction studies a much higher accuracy is required. For a given interaction time of the stored ion with the radiofrequency field, limited by the mean nuclear lifetime, this is possible by increasing the cyclotron frequency and thereby increasing the resolving power and the accuracy. This can be achieved by using highly-charged instead of singly-charged ions stored in a Penning trap. The HITRAP facility at the NESR will enable such direct mass measurements on unstable nuclides with ultra-high accuracy up to $\Delta m/m \approx 10^{-10}$. However, there is a half-life limit of about 10 s, which corresponds to the time required to cool, decelerate and inject the nuclide under investigation into the precision Penning trap. Another possibility is to use higher magnetic fields for the Penning trap yielding an improvement of up to a factor of two at present technology or to split the ring electrode of the Penning trap into segments and to induce the cyclotron resonance at higher harmonics. The latter possibility has still to be investigated.

Cooling and Polarization of Ions by Laser Light

Ions stored in rings or traps can also be cooled by interaction with laser photons. This process is possible using the high interaction cross section at the resonance of ionic transitions. The possibility of increasing the beam quality of stored ions by laser cooling has been proven by experiments in the TSR ring at the MPI Heidelberg [37] and at the ASTRID ring in Aarhus [38] for low-charge, low-γ ions.

The high velocity in the SIS200 will make this method applicable to a wide range of low- and highly-charged ions, even using conventional laser sources. Laser cooling can therefore produce a variety of highly relativistic beams of very high quality without the necessity of electron cooling. A very attractive feature will be the bunch contraction of cooled ions which has also been observed at smaller storage rings. This results in an increase of the pulse intensity of ion bunches which is of particular relevance for applications in plasma physics. The cooling from a total energy spread of 10^{-4} to the final value of 5×10^{-7}, which is the laser bandwidth, requires a time of about 10 s with a conventional laser system, depending mainly on the radiative lifetime of the transition used. In some favorable cases, much faster cooling can be expected. With circularly polarized laser beams the nuclei can also be polarized. If the polarization can be maintained in the ring or at least in some part of it, such polarized and cooled beams may open up a variety of novel experiments.

Laser cooling to extremely low temperatures and a high degree of polarization is now routinely achieved in ion and neutral atom traps. It has led to the formation of Wigner crystals, the observation of a single stored ion and Bose-Einstein condensation. Even for hydrogen-like ions stored in a Penning trap as foreseen in HITRAP, a high polarization can be obtained by using the weak M1-transition since the relaxation time is very long. Cold radioactive particles nearly at rest in space with the option of nearly 100 % nuclear polarization will stimulate new experimental

approaches such as nuclear decay spectroscopy or weak interaction studies (see next Chapter).

5.1.2.4 Atomic Physics Techniques Applied to Fundamental Tests Beyond QED

The high accuracy of atomic physics techniques has led to a large number of stringent tests of fundamental laws and symmetries in physics. The high intensity of exotic particles such as radioactive ions, highly-charged ions and antiprotons as provided by the planned GSI accelerator facilities, combined with cooling, storing and polarizing devices, will open up fascinating perspectives for advanced or novel tests of those laws and symmetries.

The test of quantum electrodynamics (QED) in extremely strong fields is addressed in Chapter 5.1.2.2 and the possible tests of the Standard Model by observation of β-neutrino correlations or super-allowed $0^+ \rightarrow 0^+$ β-decays are discussed in Chapter 1.1 of this Section 2. This Chapter will focus on novel atomic physics techniques applied to fundamental tests (except of QED) which provide unique conditions for such investigations. These are:

- Cooling of neutral atoms by laser radiation to nK temperatures.
- Cooling of charged particles by laser cooling or other techniques to mK temperatures.
- Storage of neutral and charged particles for long periods of time.
- A high degree of nuclear polarization by optical pumping.
- Easy manipulation of quantum states by radiofrequency and laser radiation.

These novel techniques, as well as the progress to be expected in the years before the powerful new GSI accelerator complex will be operational, will enable at least some of the following experiments:

- Test of symmetries (parity violation in atomic systems by neutral weak currents, nuclear anapole moment, electric dipole moment of nuclei).
- Ultra-accurate masses for the determination of the weak vector coupling constant in super-allowed $0^+ \rightarrow 0^+$ β-decays and the unitarity test of the Cabibbo-Kobayashi-Maskawa (CKM) matrix.
- Search for scalar or tensor contributions in charged weak interactions by angular correlations in β-decay.
- Comparison of gravity for matter and antimatter.
- Observation of a BCS phase transition for *fermions* in laser traps.

Although the progress in this field in recent years has been enormous, it must be emphasized that all these investigations are at the present limit of experimental feasibility.

Tests of Symmetries: Parity Violation

Atomic parity non-conservation is an important probe of the weak neutral current interactions between electrons and nucleons. The most accurate experiment [39] on atomic cesium now reaches an accuracy of about 1% and has also yielded a first measurement of the long-sought anapole moment. The dominant uncertainty stems from atomic structure calculations where correlation effects between the many electrons represent the main theoretical problem. Several proposals exist to improve the accuracy, either by measurements in different isotopes of the same element [40], by the investigation of higher-Z atoms like francium [41] resulting in a 15 times larger "weak charge" Q_w as compared to cesium, or by the use of helium-like ions [42 and references therein]. All these three suggestions involve the use of accelerators in order to deliver the required samples. Pilot experiments have already been performed at Stony Brook [41].

The proposed experiments on neutral atoms of the alkali elements make use of a magneto-optical trap (MOT) which could be coupled to the gas cell to be installed behind the new fragment separator (Super-FRS). After stopping, the ions are neutralized on a hot surface and laser cooled in the MOT. By measuring the parity-nonconserving effect in different hyperfine levels, the tiny differences in the magnitude of this effect allow for the determination of the anapole moment.

In highly-charged ions precise calculations of the atomic structure can be performed. In addition, there are near degeneracies of levels of opposite parity. The most advantageous situation occurs in heavy two-electron ions due to the near degeneracy of the two excited levels, the $^3P_0$ and the $^1S_0$ state with opposite parity around Z = 64 and Z = 92 (see Figure 5.15). In isotopes with non-zero nuclear spin the hyperfine and weak quenching effects are mixed. This leads to an unusually large asymmetry of the delayed photon emission by polarized ions which can be measured in beam-foil type experiments [42]. The potential of the planned new GSI facility for these studies is evident since the near degeneracy between the $^3P_0$ and the $^1S_0$ states depends sensitively on the nuclear size effect. Therefore, the parity violating effects can get strongly amplified by choosing isotopes with the smallest possible energy spacing.

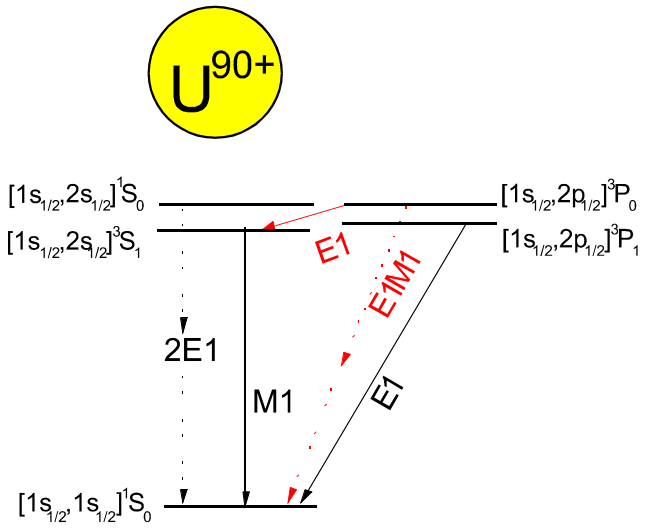

Figure 5.15: Level scheme of the first excited states in helium-like uranium. For U^{90+} a near degeneracy between two L-shell levels with opposite parity occurs (the $^3P_0$ and the $^1S_0$ state), making this system well suited for the search of parity violation in atomic systems.

Test of Symmetries: Nuclear Electric Dipole Moment

The assumption of the invariance of physical processes under a combined charge conjugation (C), parity (P) and time reversal (T) transformation forms the CPT theorem which is ranked among the most basic principles in modern physics. The existence of a permanent electric dipole moment (EDM) of elementary particles, nuclei and atoms would violate both P and T invariance. Provided CPT symmetry is rigorously valid, the observation of an EDM would also violate the combined CP symmetry. Based on the observed CP violation in the neutral kaon system, predictions for the EDM of elementary particles like leptons and nucleons can be made in the framework of the Standard Model. The resulting value for the neutron is about 6 orders of magnitude below the current experimental limit of 6.3 x 10^{-26} e cm [43]. For the electron EDM the Standard Model prediction is many orders of magnitude below the present limit of 1.8 x 10^{-27} e cm [44]. However, a variety of speculative theories, which try to explain some of the shortcomings of the Standard Model, yield EDM predictions that are as large as these bounds.

GSI offers a worldwide unique combination of opportunities to develop, set up and carry out a most sensitive and competitive search for the EDM of nuclei. It exploits particularly the high particle fluxes that are available for stable and radioactive nuclides and the small phase space achievable for them [45].

Searches for permanent nuclear EDM receive a strong motivation from the very unsatisfactory situation in the big bang-based standard cosmology. The underlying theoretical framework assumes the temporal constancy of fundamental constants and ascribes the observed matter/antimatter asymmetry to CP violating forces. The CP violating processes discovered up to now are by far not sufficient to support this model of matter genesis. Therefore sensitive searches for new sources of CP violation [46] are highly desirable. A regular enhancement of the EDM of a nucleon by about one to

two orders of magnitude can be expected to arise in large nuclei [47] from CP-odd nuclear forces. Searches in heavy nuclei are particularly promising, if a sensitivity beyond 10^{-25} e cm can be reached.

For an elementary particle, the magnetic moment $\vec{\mu}$ and any hypothetical EDM $\vec{d}$ are proportional to the angular momentum $\vec{J}$:

(5.5)
$$\vec{\mu} = g \cdot \frac{Ze\hbar}{2m} \cdot \vec{J} \quad and \quad \vec{d} = \eta \cdot \frac{Ze\hbar}{2mc} \cdot \vec{J}$$

Here, *Ze* is the charge, *m* the mass, *g* the magnetic *g*-factor and η its electric counterpart which carries the interesting part of the new physics being searched for. In an external magnetic field $\vec{B}$ the particle performs a Larmor spin precession around the magnetic field axis and in an external electric field $\vec{E}$ an independent analogous precession around the electric field axis with the respective frequencies:

(5.6)
$$\vec{\omega}_m = \frac{\vec{\mu} \cdot \vec{B}}{\hbar} \cdot \frac{\vec{B} x \vec{J}}{\left|\vec{B} x \vec{J}\right|} \quad and \quad \vec{\omega}_d = \frac{\vec{d} \cdot \vec{E}}{\hbar} \cdot \frac{\vec{E} x \vec{J}}{\left|\vec{E} x \vec{J}\right|}$$

An electric-field dependent spin rotation will therefore reveal any EDM. This concept has been employed in all sensitive EDM searches to date.

A novel method for EDM measurements could be envisaged as follows (Figure 5.16). Longitudinally polarized highly-charged heavy ions with velocities $\beta = v/c \geq 0.2$ are injected into a weak focusing magnetic storage ring with a typical field strength B > 1.5 T where they experience a motional electric field up to about 100 MV/cm. In the magnetic field the ions will rotate at the cyclotron frequency. The spin will precess faster by the anomalous frequency given by:

(5.7)
$$\vec{\omega}_a = \frac{g-2}{2} \frac{\vec{\mu} \cdot \vec{B}}{\hbar} \frac{\vec{B} x \vec{J}}{\left|\vec{B} x \vec{J}\right|}$$

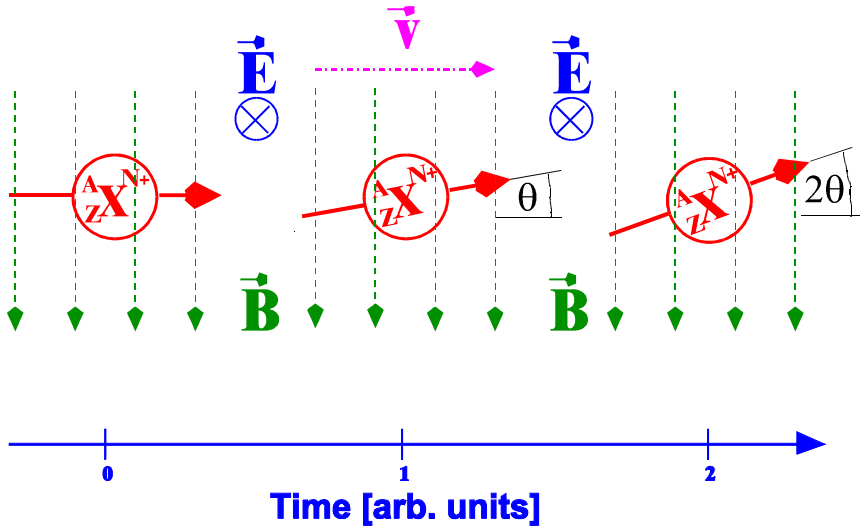

Figure 5.16: The basic principle of the proposed novel experimental scheme. Relativistic heavy ions ($^{A}_{Z}X^{N+}$) of velocity $\vec{v}$ moving in a magnetic storage ring with field $\vec{B}$ are exposed to a motional electric field $\vec{E} = \vec{v} \times \vec{B}$. In case of a finite small EDM and compensated magnetic anomaly spin rotation, the nuclear spin precesses with a linear increase of the angle θ with increasing time.

In case of a finite EDM the spin will precess at the frequency $\vec{\omega}_a + \vec{\omega}_d$. The EDM manifests itself in a time-dependent vertical component of the polarization. This principle has been utilized in EDM experiments on the muon at CERN and at BNL. The new concept [48] introduces a radial electric field which translates into a motional magnetic field for the stored particles. It can be adjusted to compensate the magnetic anomaly precession. Then, a vertical polarization will appear which increases linearly with time. The compensation effect is inversely proportional to the momentum spread of the stored ions.

To significantly surpass current neutron results, a reliable search for nuclear EDM should be sensitive to better than $\eta = 2 \times 10^{-11}$. To achieve this goal, about 2×10^{9} appropriate ions should be provided, that have to be longitudinally polarized as well as momentum-cooled. For this purpose, the new GSI facility offers considerable advantages: all kinds of electron-cooled heavy ion beams will be available there, including some fully stripped ions such as ^{223}Fr [49], or ions with partly filled atomic shells such as $^{141}Cs^{49+}$, where the magnetic moment can be 'adjusted' by an appropriate number of electron pairs and appropriate compensation fields [50]. However, some basic issues must be addressed before such a nuclear EDM experiment can be designed in detail: a significant longitudinal nuclear polarization must be first provided, then preserved, and finally detected after an appropriate storage time in the ring.

In a recent workshop [45] various eventual solutions were discussed concerning an ample production as well as a safe and controllable maintenance of the longitudinal nuclear polarization of highly-charged ions. If these prerequisites of a nuclear EDM experiment can be solved, a very rich physics potential as well as a most interesting challenge at the forefront of modern technology are to be expected. An experiment

addressing nuclear EDM at the new GSI facilities will allow conclusions even well beyond those which have emerged from the neutron EDM searches.

Ultra-Accurate Masses for the Weak Vector Coupling Constant G_V

As discussed in Chapter 2.3 in Section 2, precise determinations of the ft-values for super-allowed $0^+ \rightarrow 0^+$ Fermi β-decays are required in order to determine accurately the weak vector coupling constant G_v and to test in this way the conserved vector current (CVC) hypothesis and the unitarity of the CKM matrix. Beside high-precision measurements of the branching ratio and of the half-life, the Q-value of the β-decay has to be determined with an accuracy of 1 keV or better, corresponding to a mass measurement of the mother and daughter nucleus at an accuracy level of 10^{-8} for mass number A = 100. Only Penning traps offer such an accuracy for radioactive nuclides by a measurement of the cyclotron frequency of the ion stored in a strong magnetic field. While the atomic mass of a stable isotope has already been measured with an accuracy of up to $\Delta m/m = 10^{-10}$ [51], on-line Penning traps such as ISOLTRAP have presently reached an accuracy of up to 10^{-8} for nuclides with a half-life of 1 s, as recently confirmed by use of carbon clusters. Further development is required in order to maintain this accuracy for the case of mass measurements of nuclides with half-lives much shorter than 1 s (see Chapter 5.1.2.3). Recent mass measurements with ISOLTRAP on ^{33}Ar ($T_{1/2}$ = 174 ms) with an accuracy of 1 x 10^{-7} and on ^{74}Rb ($T_{1/2}$ = 65 ms) with an accuracy of 3 x 10^{-7} [52] indicate that these goals seem realistic.

Search for Scalar or Tensor Contributions in the Charged Weak Interaction by Angular Correlation in the β-Decay

In the framework of the Standard Model, nuclear β-decay is described by the virtual exchange of W bosons which have vector and axial vector couplings. In theories which go beyond the Standard Model, however, the existence of scalar and tensor couplings in weak interaction is predicted. A search for such scalar and tensor currents can be made in measurements of the beta-neutrino (β-ν) correlation in pure Fermi or Gamow-Teller decays. Since the neutrino cannot be directly detected, the correlation between the β-particle and the recoiling daughter nucleus has to be measured.

Ion traps and neutral atom traps offer optimum conditions for those experiments. Both types of traps provide:

- A well localized small source of radioactive ions or atoms.
- The decaying nucleus in a material-free environment (no source scattering, direct detection of the recoil ion), and the possibility of polarizing the mother nucleus.

Laser traps can confine a highly-polarized sample of atoms and can reach high atom densities [53] but have the disadvantage of being essentially restricted to isotopes of alkali elements. Ion traps are generally applicable, but have lower ion density and make the observation of the recoil ion difficult due to the constant (Penning trap) or time-varying (Paul trap) electromagnetic fields.

Table 5.2 lists the activities performed worldwide in weak interaction studies using trapped ions or atoms. Neutral atom traps for radioactive species are mainly operated in North America whereas ion traps for nuclear physics seem to be more a European specialty. There is a strong expertise in ion trap physics at GSI which was transferred within the TMR Networks EUROTRAPS and EXOTRAPS (funded by the European Commission) to quite a number of universities and research institutes.

It can be expected that at the planned GSI facilities the "free choice" of a nucleus suited for weak interaction studies and the available high intensities of radioactive beams will make a strong impact on this challenging field, allowing to address items such as ($\vec{J}$ = nuclear spin vector, $\vec{p}$ = beta particle momentum, $\vec{q}$ = neutrino momentum, $\vec{s}$ = polarization of beta particle):

- The beta asymmetry parameter A (i.e., the $\vec{J} \cdot \vec{p}$ correlation), sensitive to right-handed and tensor currents.
- The longitudinal polarization of beta particles emitted by polarized nuclei, sensitive to scalar and right-handed currents.
- Triple correlations such as $\vec{J} \cdot (\vec{p} \times \vec{q})$, or $\vec{S} \cdot (\vec{J} \times \vec{p})$, sensitive to, e.g. violation of time-reversal invariance.

Table 5.2: Ion or atom traps in operation (op.), under construction (uc.), or planned (pl.) for weak interaction studies. The main isotopes under investigation are indicate and the scientific goals and the applied trap technology are listed.

Isotope	Goal	Institute	Kind of Trap	Status	Ref.
^{6}He	β-ν correlation	GANIL, Caen	Paul trap	uc.	[54]
^{14}O	β-ν correlation	ANL, Argonne	Paul trap	uc.	[55]
^{14}O	β-ν correlation	LBNL, Berkeley	Paul trap	uc.	[56]
^{20}Na, ^{21}Na	β-asymmetry	KVI, Groningen	atom laser trap	pl.	[57]
^{21}Na	β-asymmetry	LBNL, Berkeley	atom laser trap	op.	[58]
^{35}Ar	β-ν correlation	ISOLDE/CERN	Penning trap	uc.	[59]
^{37}K	β-asymmetry	TRIUMF, Vancouver	atom laser trap	op.	[57]
^{38m}K	β-ν correlation	TRIUMF, Vancouver	atom laser trap	op.	[57]
^{82}Rb	β-asymmetry	LANL, Los Alamos	atom laser trap	op.	[53]
^{210}Fr	parity violation	Stony Brook	atom laser trap	op./pl.	[57]
^{211}Fr	parity violation	JILA, Boulder	atom laser trap	op./pl.	[60]
^{210}Fr	parity violation	INFN, Legnaro	atom laser trap	uc.	[61]

Comparison of the Gravitational Force for Matter and Antimatter

The planned new GSI facility will be worldwide the most intense source of low-energy antiprotons. The beam intensity of extracted low-energy (about 5 MeV) antiprotons will be two orders of magnitude higher at the NESR compared to the Antiproton Decelerator (AD) at CERN, which is a dedicated machine for CPT tests on antihydrogen and for low-energy antiproton collision experiments. Hence, it can be anticipated that experiments with trapped antiprotons can be performed at a NESR trap facility which, due to intensity reasons, are currently impossible anywhere else. A highlight would be the first direct experimental investigation of the gravitational interaction of antimatter that has never been attempted up to now. Such investigations could be performed on antihydrogen atoms which might be produced by recombining trapped antiprotons with positrons [62] in a so-called nested trap. The effect of gravity on antimatter is an important issue for the development of quantum theories of gravity [63].

Bardeen-Cooper-Schrieffer (BCS) Phase Transition of Radioactive Atoms in Laser Traps

In recent years, the experimental investigation of Bose-Einstein condensation (BEC) at ultra-low temperatures in laser traps has received great attention worldwide [64] and was honored with the physics Nobel Prize for 2001. In these experiments, the trapped atoms are bosonic particles ^{1}H, ^{7}Li, ^{23}Na or ^{85}Rb. A novel development in this field of quantum degeneracy are experimental attempts to create a condensate of *fermionic* particles. The scientific significance of such a Bardeen-Cooper-Schrieffer (BCS) phase transition is comparable to the observation of BEC.

A promising approach towards the first observation of a BCS phase transition are laser trap experiments with unstable isotopes which obey Fermi-Dirac statistics. There are several candidates for BCS condensation, for example ^{84}Rb which is particularly well suited for these studies. Trapping, laser cooling and evaporative cooling of neutral atoms is state of the art in today's BEC experiments. An important technique for achieving BCS condensation is the possibility to fine-tune the fermion-fermion coupling strength. This tuning is accomplished by manipulation of certain atomic energy levels (Feshbach resonances) via the magnetic-field strength in the neutral-atom trap. Also the sympathetic cooling of two simultaneously trapped atom species [65] could be an important ingredient for BCS condensation as demonstrated recently with trapped ^{85}Rb and ^{87}Rb atoms [66].

The radioactive atoms which are needed for experiments on BCS condensation of fermionic systems can be produced at high rates at the future GSI accelerator facility. These challenging experimental studies of quantum degeneracy for fermionic systems will complement the experimental program of weak interaction studies with laser-cooled atoms in neutral-atom traps described above.

5.1.2.5 Ions and Electrons in Ultra-High Intensity, Femtosecond Laser Fields

A new field of research will be opened by the combination of ultra-intense laser pulses and highly-charged ions. In the strong electric field created in the focus of ultra-high intensity lasers, as shown in Figure 5.17, the Coulomb potential of atoms or low-charged ions is sufficiently depressed to allow bound electrons to escape over the potential barrier or to tunnel through it [67].

This is not the case for heavy highly-charged ions where the binding field strength is still much higher than the applied field strength produced in the focus of the most intense present-day lasers (see Figure 5.3). Distinctly different from the case of low-charged ions, multi-photon processes induced by the intense laser field do not saturate by the inset of field ionization. Consequently, high-Z ions will allow one to enter a completely unexplored regime for the study of the interaction of intense laser fields with matter.

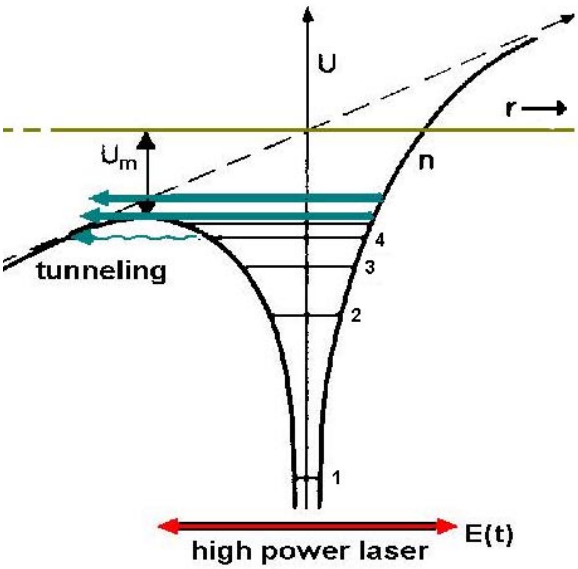

Figure 5.17: Atoms and moderately charged ions are readily field-ionized on a femtosecond time scale in ultra intense laser fields. In the focus of a petawatt laser with an intensity of 10^{21} Watts/cm² an electrical field of 10^{12} V/cm is reached. Because this induces a potential depression U_m of several keV, it normally leads to instantaneous field ionization.

Hard X Rays

In the intense field of a laser, atomic electrons are subject to violent accelerations and may reach highly relativistic velocities. The re-scattering of such electrons in the field of the nucleus leads to the generation of high-energy photons up to, or even beyond the photoionization threshold. The photon energies produced by this high-harmonic generation will even be sufficient to excite the nucleus.

In addition, a related and very interesting research topic is the direct interaction of the accelerated electrons with the nucleus or, in the case of few-electron ions, with other bound electrons. In particular, one expects that the presence of an applied strong laser field will drastically modify the dynamics of electron capture and

ionization processes, which will affect for example the stopping power of relativistic ion beams.

A bunched electron beam of high brilliance as proposed for the electron elastic scattering experiments will add the possibility of experiments using hard x-rays generated by laser-electron scattering. In the geometry shown in Figure 5.18 intense laser pulse impinging head-on onto the electron beam will effectively produce an undulator field for the electrons [68] which leads to the emission of two-fold Doppler shifted energetic photons. The number of energetic photons produced this way is close to the number of electrons in the bunch of the electron beam if the two pulses match in time and are comparable to the interaction length. The intrinsic width of the produced x-ray pulse is inversely proportional to the number of wavelengths in the pulse.

For the case of good beam quality, as also required for the scattering experiments, a 10^{-3} energy resolution can be expected at 3 ps pulse length for a laser wavelength of 1 µm, e.g. the PHELIX laser. The kinematic situation provides very intense, short pulses of hard x-rays with an energy of

(5.8)
$$E_{x-ray} \approx 4 \cdot \gamma^2 \cdot E_{Laser} .$$

For electron energies of 150 MeV, bunches of 5 x 10^{10} electrons, and laser pulses of 10 Joule energy both with 3 ps duration, this produces pulses of more than 10^{10} photons with energies of 360 keV in pulses comparable to the bunch length of the electrons. With the proposed geometry where the electron beam merges with the ion beam, the created photons will also perfectly overlap with the ion beam. This gives direct access to the spectroscopy of hydrogen-like systems, the excitation of low-lying nuclear states, and the creation of electron positron pairs.

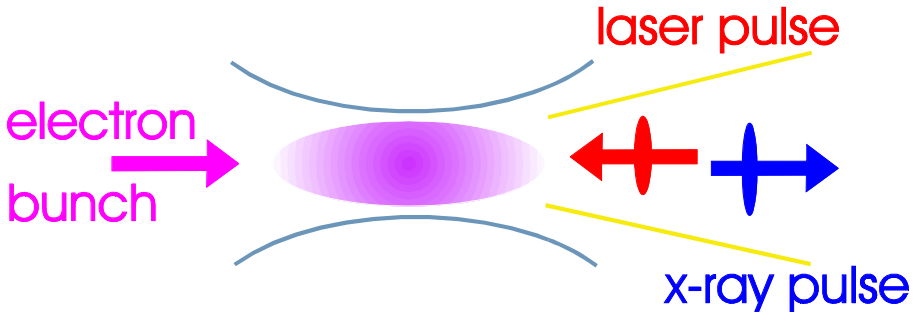

Figure 5.18: Laser pulse ($E_{Laser} \approx 1$ eV) impinging head-on onto a 150 MeV electron beam ($\gamma \approx 300$), whereby backscattered photons of an energy $E_{x\text{-}ray} \approx 4\gamma^2 \approx 360$ keV in the laboratory are created.

5.1.3 Interaction of Relativistic Heavy Ion Beams for Materials Research

Energetic heavy ions traveling through a solid exert an enormous electric field (of order 10^{12} V/m) over an extremely short time period (some 10^{-18} s or even less) at the site of constituents (atoms, electrons, etc.) of the solid in close proximity to the trajectory, thereby transferring kinetic energy. This energy loss triggers very complex, rapid processes, beginning with the generation of fast electrons, followed by Coulomb repulsion of the ionized atoms, by x-ray and Auger electron emission, electron-phonon coupling, etc. As a final result, the projectiles cause long, narrow modified zones with radial extensions of a few nanometers. Due to their macroscopic length, they are quasi-one-dimensional perturbations of the solid. In many materials, dramatic modifications are induced such as phase changes inside the track cylinders from the crystalline to the amorphous state or from a superconductor to an insulator, and the creation of a high temperature or high pressure phase. The track features constitute signatures of the specific properties of a given solid and reveal, in which way this solid copes with the deposition of energy under extreme conditions [69].

Modifications induced by ions of a total kinetic energy up to several GeV are one of the subjects continuously studied in materials research. There exists a large amount of experimental data on tracks in different classes of solids, such as polymers, metals, ionic crystals, and some selected semiconductors, to name a few. These radiation-induced defects have been analyzed with a variety of methods including high-resolution microscopy, optical spectroscopy, x-ray and neutron scattering, etching, nanoprofilometry, Rutherford backscattering, and others. Furthermore, the experimental findings were accompanied by the development of theoretical concepts concerning the mechanisms of track creation. The thermal spike and the pressure pulse model may be mentioned here as prominent examples.

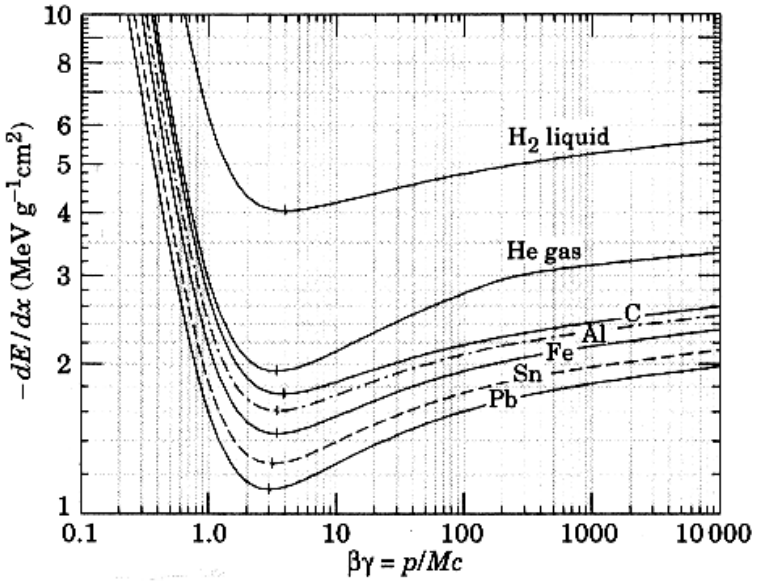

Figure 5.19: Energy loss dE/dx of protons in matter as a function of their generalized velocity, $\beta\cdot\gamma$[70].

The most important quantity for track formation is the stopping power dE/dx (energy loss per unit path length) of the projectile. The stopping mechanisms are rather well understood for non-relativistic energies. As the ion velocity increases to relativistic values, dE/dx decreases reaching a minimum at about 2 GeV/u. For even higher ion energies, new phenomena set in due to relativistic effects, and the stopping power increases again slightly (Figure 5.19). Comprehensive experimental dE/dx studies have been performed at projectile energies in the range ≤ 1 GeV/u [71-75]. In contrast to that, only scarce quantitative experimental dE/dx data is available to date above 1 GeV/u (a single data point existing for 160 GeV/u Pb ions [76,77]). The understanding of basic energy loss processes at extremely high beam energies [78,79] must be improved by new experiments using different kinds of materials.

Besides the magnitude of dE/dx, the energy density plays a crucial role for track creation. For higher ion velocities, energetic knock-on electrons distribute their energy radially in a larger cylindrical volume. Therefore, the energy density per atom (or energy per lattice plane) decreases (Figure 5.20). For applications in material modifications, the energy density effect of such energetic ion projectiles is not known. At ultrahigh ion energies, tracks in very sensitive materials (e.g. polymers) may be enlarged, whereas in resistant materials, the critical energy density is not surpassed and track formation is suppressed.

Track formation processes and defect characteristics at the conceived beam energies and intensities are also important for the suitability of different materials in accelerator facilities, experiment setups, and for the development and improvement of detectors. Based on the high energies and small stopping powers, the new ion beams have much larger penetration depths. Novel types of experiments will become possible.

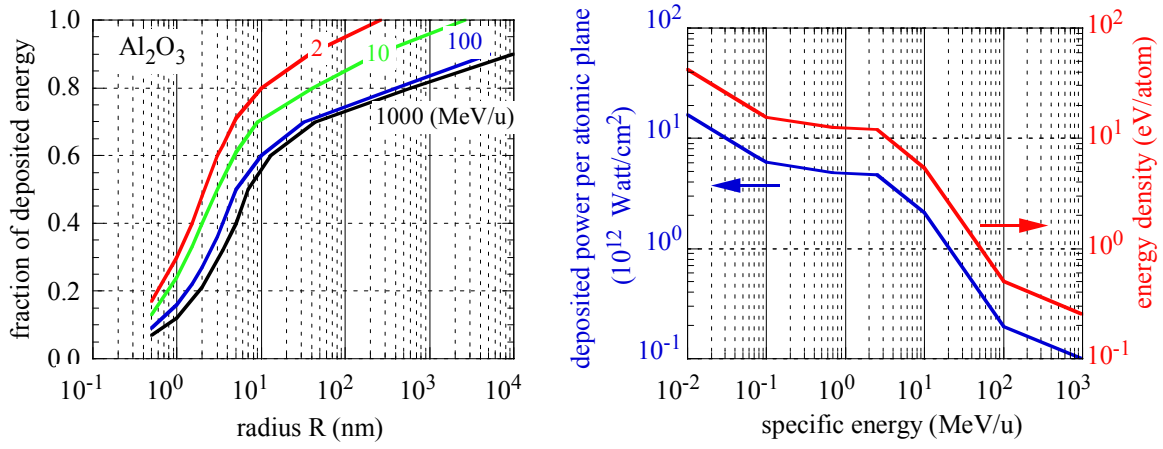

Figure 5.20: Effect of ion velocity on radial energy density;lLeft: Fraction of energy deposited in a cylindrical region of radius R for low and high ion energies;
right: Energy density (eV per atom) and power transfer per lattice plane (Watt/cm²) versus specific ion energy.

Material Modifications

When a high-energetic ion beam passes through a target, the stopping power increases until it finally reaches the Bragg maximum close to the end of the path, where the ions come to rest. In general, a critical energy loss is required to induce modifications in a specific material. This property can be used to create buried regions of local structural changes embedded deeply in the otherwise unmodified target (Figure 5.21). In complex devices, e.g. inner walls with etchable tracks or buried amorphous layers can be created.

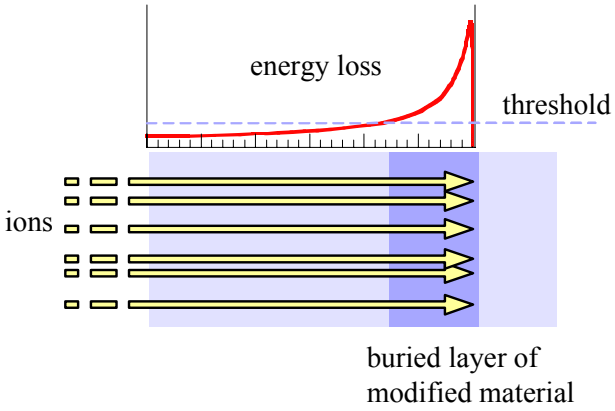

Figure 5.21: Creation of a buried layer with modified properties depending on the damage threshold of different materials.

Radiation-sensitive materials (low threshold) can be modified with rather uniform energy deposition over large distances along the ion trajectories by placing the Bragg peak of the energy loss curve outside of the target. Using radioactive beams available at the new facility, radioactive probe ions can be deposited in a target depth far from the surface and unreachable by other techniques.

Irradiation of Larger Devices

Based on the long projectile range, high-energy ion beams will allow the irradiation of complex experimental setups. Radiation sensitivity and damage due to relativistic projectiles at different locations and depths can be tested for larger devices such as complete satellites, large spacecraft components, or entire detector setups.

The new facility offers the possibilities of carrying out experiments under extreme conditions such as track formation in a pressurized sample in a diamond-anvil cell [80]. Such high-pressure investigations are of great relevance in the field of geochronology and geophysics where tracks of fission fragments are commonly used for dating [81]. Although there are indications for the influence of pressure [82], heavy-ion experiments in a special pressure cell have not yet been possible due to the larger dimensions and the required ion ranges and fluences. At the new facility, the

pressure cell can be exposed to the ion beam tuning the energy in a way that the highest energy loss (Bragg-peak) occurs in the sample under investigation.

Observation of Transient Processes

For a better understanding of the track formation mechanisms, it is extremely important to investigate transient processes taking place during or shortly after the passage of the ion projectile (Figure 5.22). Electronic processes dominate the track evolution on a time scale from roughly 10^{-18} to 10^{-13} s. The dynamics of damage production on the scale in the order of 10^{-14} s can be studied by high-resolution convoy- and Auger electron spectroscopy [83,84] as well as by x-ray detection. However, these short-time techniques yield information on the heating up of the electrons in the bands before the atoms are set in motion and therefore do not give a complete picture of the track formation mechanisms. The movement of the atoms resulting from the high electronic excitation typically occurs on a time scale of 10^{-13} to 10^{-12} s, but also includes slower processes related to the cooling of the lattice or, for example, on shock wave propagation. The creation of a shock wave as a consequence of the projectile passage can be studied in solid targets by monitoring ultrasonic signals (pulse width between 3 and 600 ns) by means of piezoelectric sensors [85].

The beam parameters of the new facility, in particular the combination of much higher intensities and shorter ion pulses will allow to access fast processes. Such experiments require a time definition of an incoming single ion in the order of 10^{-11} s or shorter and a high temporal resolution of signal diagnosis. Access to extremely rapid processes could be obtained by collecting the Cerenkov light produced by ultrarelativistic ions. The collected light is auto-synchronized with the transient track processes and can be used to directly probe modifications induced in the solid by monitoring transient changes of transmission, reflectivity or scattering of diffuse light on the target surface similar to the technique applied in pump-probe laser experiments. But also on a much slower time scale (10^{-9} s) there exist in specific materials interesting processes, for example radical reactions in polymers (Figure 5.22).

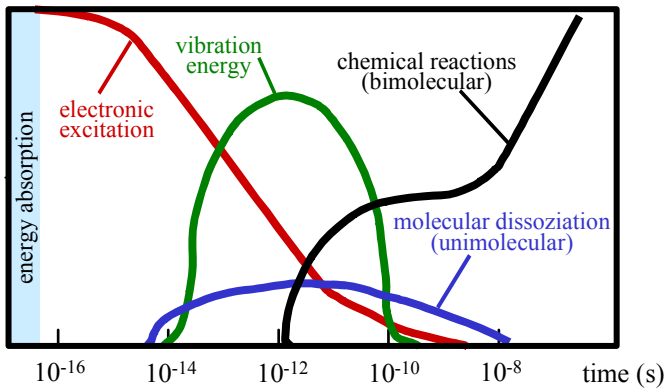

Figure 5.22: Scheme of energy dissipation as a function of time after ion impact in polymers.

In numerous dielectrics, swift ions induce luminescence originating from excited states of electron-hole pairs (so-called excitons). Using single-ion hits and single-photon counting, luminescence detection is an extremely sensitive technique and allows measurements at energy loss values as low as 0.2 keV/nm [86]. Studies of the luminescence originating from excitation by relativistic ions in dielectrics improve the understanding of the ion stopping process in matter and are also of interest for developing new fast scintillators.

Experiments can be performed with high intensity ion pulses but also by collecting the signal along the extremely long path of single ions. For high beam intensities, the regime from single thermal spikes, to collective effects of many ions up to the transition to the hydrodynamic plasma situation can be tested. In this respect it is also planned to use the PHELIX laser system which is designed to serve as x-ray source generating multiple laser pulses of sub-ns duration.

5.1.4 Application of Relativistic Ions in Radiobiology and Space Research

Solar and cosmic radiation represent a major hazard in all space explorations [87, 88]. In mankind, genetic alterations and cancer may already be induced by low levels of radiation. In the case of a solar flair event, a lethal dose can be delivered to men within only half an hour of exposure or even less. For computer chips and other electronic devices, the high charge locally deposited by energetic heavy ions can produce alterations in the semiconductors and change the status of a memory. In extreme cases when showers of particles are involved information can get lost completely and stopping heavy particles can destroy semiconductors permanently.

Because in space shielding is difficult and costly, the action of the cosmic radiation should be known as precisely as possible in order to reduce shielding to the necessary minimum [89]. Whereas the solar particle stream mainly consists of protons and helium ions, the cosmic radiation has a significant component of heavier ions up to iron (Figure 5.23) [87,88].

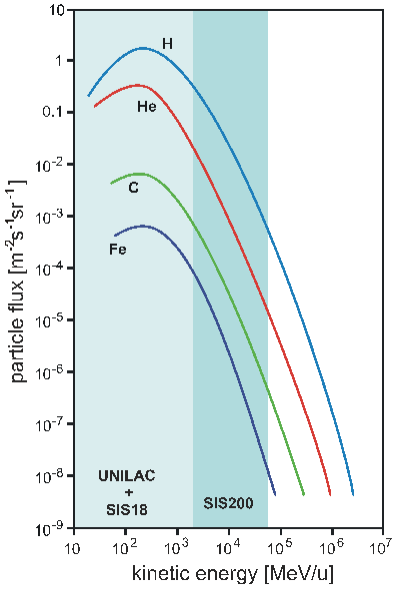

Figure 5.23: Energy spectrum of the particles in galactic cosmic radiation.

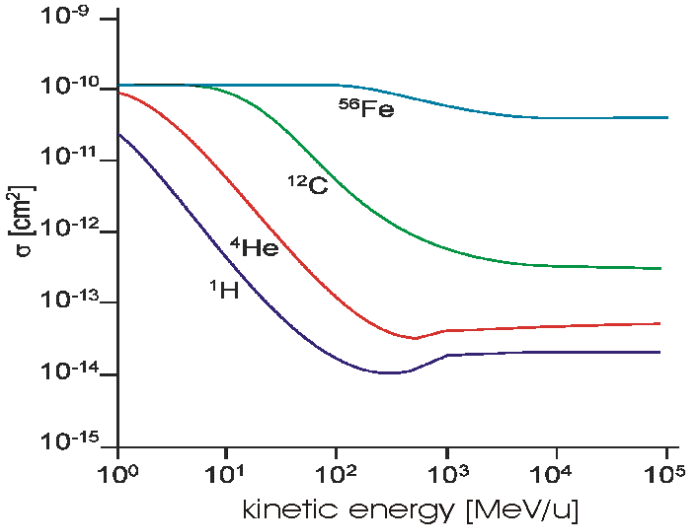

Figure 5.24: Calculated risk coefficient for the induction of transformations of mammalian cells as a model of the expected influence of cosmic radiation for long-term effects. This model calculation contains also the influence of nuclear fragmentation (according to [89]).

Beyond iron, the intensity becomes very low. For both effects, damage in biological material as well as in electronic devices the dose is the determining factor. First, this is the dose in a macroscopic way as defined as the energy deposition per mass unit in macroscopic volumes, but even more important is the dose in a microscopic way as the local dose distribution inside individual particle tracks.

The energy loss of particles is given by the Bethe-Bloch-formula and depends on the square of the atomic number. Therefore, the macroscopic dose from the heavy

components of cosmic radiation like iron is not negligible compared to the dose from light ions although heavier ions are less frequent than lighter ones (Figure 5.24). But more important than the macroscopic dose is the microscopic dose inside a track [90]. The local dose of an individual particle reaches values of many kilo-Gray in the center of a track. In microscopic fields of such high dose levels, an increase of the efficiency more than proportional to the low dose response has been observed for many biologic objects. Because damage is produced in close proximity for instance at both DNA strands the lesions can interact and potentiate their biological relevance producing the observed elevated Relative Biological Efficiency (RBE) [91, 92]. Taking the RBE effect as well as the fragmentation into account the cross sections for cell transformation of Fe are much larger than for protons (Figure 5.24) and compensate the difference in abundance. At energies significantly above 1 GeV/u the cross section should level off due to the influence of fragmentation products, but these calculations have not been confirmed experimentally.

For ions with energies in the range of the new accelerator, there are no systematic measurements concerning biological or physical efficiency. It is also impossible to predict the effect of these ions only from an extrapolation from lower energies. At energies higher than 1 GeV/u the radiative energy loss becomes relevant in addition to the electronic energy loss. More interesting, however, might be the fragmentation process where the projectile produces lighter fragments emitted in a small cone in forward direction. This fragmentation process is the reason why shielding with thick layers of material does not reduce the dose: while low-energy ions are stopped in the shielding material, high-energy particles produce showers of low-energy particles of high dose. Moreover, the fact that these particles are correlated and occur simultaneously raises the question of proximity effects, not necessarily at DNA level but possibly at higher levels of organization such as cells or tissues. The same is true for semiconductor chips: correlated damage might be more efficient than that of single individual ions. In order to test this hypothesis biological experiments on cellular level exploring genetic effects should be performed first [93, 94] and should be completed by some tissue experiments later on. Furthermore, it is necessary to test electronic components for space flight for the influence of high-energy cosmic rays.

Both types of experiments require an irradiation facility where the beam can be enlarged either by scattering foils or by the employment of a scanning system. Both systems for beam enlargement are necessary. The scanning system [95] offers homogeneous particle fluences over large areas which is a big advantage for most irradiation experiments. In addition, the scanned beam is not contaminated with secondary fragments. On the other hand, a scattering system allows to study moving targets like cells in a centrifuge at elevated g-values which offers the opportunity to study the possible influence of gravitation effects on biological repair. These experiments require a representative set of ion beams from protons to uranium with fluxes in the order of $10^3 - 10^{10}$ cm^{-2} s^{-1}.

5.2 Instrumentation and Detectors

5.2.1 Experiments at SIS200

In-Ring Laser Experiments and Laser Cooling

Due to the high value of γ, in SIS200 direct laser excitation of Li-like heavy ions becomes possible. The principal arrangement for laser cooling and in-ring laser experiments are conceptually equivalent.

In-ring laser spectroscopy has already been performed in several cases successfully at the ESR [28,29]. The requirements in general are

- An interaction region of 5 to 15 meters where ions and laser beam can be overlapped.
- A detection device to observe photons generated by laser excitation.
- A laser laboratory (100 m^2) close to a straight interaction zone but outside of the radiation hazard.

At the ESR the merging of the laser beam with the ion beam was accomplished in the straight sections between the deflection magnets, the laser entering and exiting through the straight ports of the dipoles. This will not be practical with the superconducting-magnet technology at SIS200. As a compromise, a small angle between the beams has to be tolerated. In a straight forward manner, maintaining the full aperture of the SIS200 beam line, and using the space within the two outer quadrupoles of a triplett, the angle would be 2.7 mrad. A smaller crossing angle is accomplished if the mirrors for the laser are moved closer to the beam axis for the actual experiments. The laser beam will typically be injected anti-parallel to the ions, in order to make use of the large Doppler boost. The positions of both beams have to be controlled accurately at all times. At the ESR good results were obtained with a set of mechanical scrapers, which allows for a direct comparison of the relative position of ion and laser beams. Alternative methods are explored at other storage rings, using non-destructive position sensors for the ion beam.

Due to the large Lorentz factor of $\gamma \approx 23$, projectile photon emission appears strongly enhanced at forward angles in the laboratory. This demands that x-ray detection should be as close as possible to the beam axis, similar to the requirements for the laser beam.

The laser laboratory has to be reasonably close to the experiment, although distances of up to 100 meters can be tolerated for a laser beam line. Special installations must be foreseen to allow for remote control of the experiments.

Experiments Using Slow-Extracted Ion Beams

The experiments in the fields of atomic physics, radiobiology, and materials research to be performed at a new experimental area using alternatively SIS18 and SIS200 beams will concentrate on atomic structure and collision studies at moderate and high-relativistic energies as well as on irradiation of individual samples for biological or solid material research. In addition, it is planned to test the radiation sensitivity of large electronic components (e.g. microprocessors) of space crafts, and to calibrate detector systems for cosmic radiation studies. The overall properties and geometrical dimensions of this experimental area will be very similar to the existing Cave A at SIS18 (see Figure 5.25).

For the irradiation facility used by radiobiology and to be installed in the new cave, slow-extracted beams of protons up to uranium ions are available with a flux ranging from $10^3 - 10^{10}$ $cm^{-2}s^{-1}$. For biology experiments with typical sample areas of 150 cm^2 dose rates of about 5 Gy/min are required. The corresponding particle fluxes for various ion beams at 3 GeV/u are shown in Table 5.3.

For homogeneous irradiations of larger samples, a magnetic beam scanner is foreseen (see Table 5.4). The desired scan speed of 1 cm/ms can be achieved for magnetic rigidities up to about 50 Tm with tolerable eddy-current losses. At higher rigidities sample moving techniques have to be used for long-area irradiations. In addition, a scattering system will provide statically defocused beams.

Table 5.3: Particle flux requirements for biology experiments.

Ion	**Flux [$cm^{-2} \times s^{-1}$]**
p	4 x 10^{10}
He	1 x 10^{10}
C	1 x 10^{9}
O	7 x 10^{8}
Ne	4 x 10^{8}
Ar	1 x 10^{8}
Fe	6 x 10^{7}
Kr	3 x 10^{7}
Xe	1 x 10^{7}
U	5 x 10^{6}

Table 5.4: Properties of the magnetic beam scanner system

Ion stiffness:	20 - 50 Tm
Scan area:	10 x 10 cm^2
Distance (magnet-sample):	10 m
Scan rate:	ca. 1 cm/ms
Beam diameter:	ca. 5-10 mm

The samples are placed into the beam position by a remote control robot or with linear transport systems.

Various parameters during the irradiation procedure are monitored by similar techniques as in the existing cave A. To control the position and the intensity of the beam over a wide intensity region, detectors such as ionization and multi-wire chambers are used. For the controlled application of a given fluence, the extraction from SIS200 has to be interrupted fast enough.

Besides the irradiation facility itself, extra space is needed for in-beam experiments requiring e.g. a vacuum chamber, a high-pressure cell, or a centrifuge for biological cells. To observe specific processes during or shortly after the ion passage through matter, in-situ monitors (e.g. spectrometers) are planned. In particular for radiation biology, an x-ray beam for comparative studies has to be available in or near the new cave.

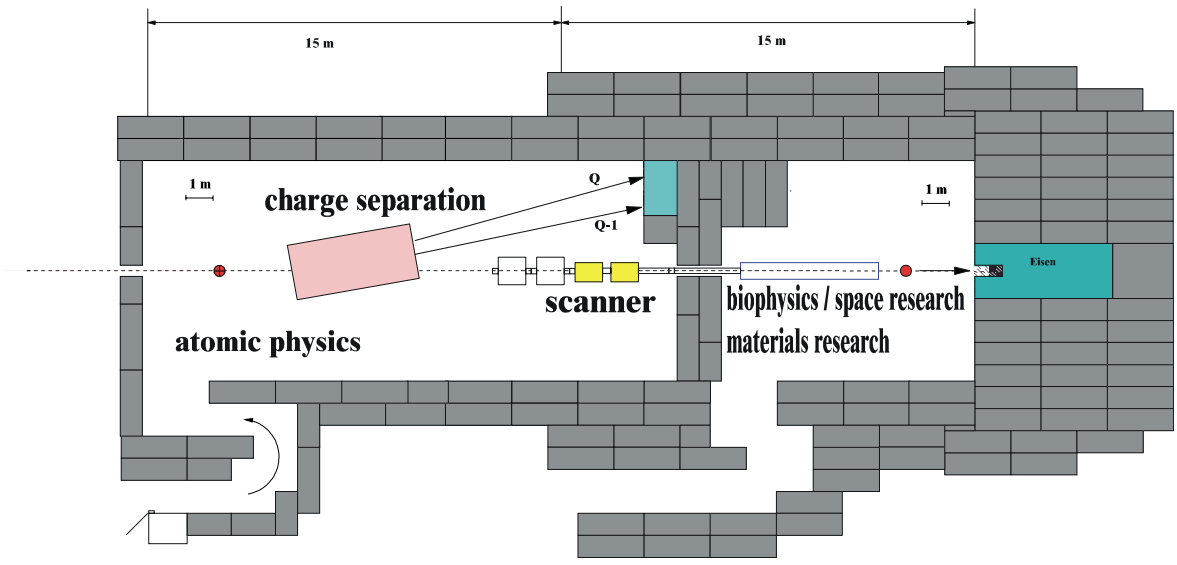

Figure 5.25: Experimental area for atomic physics, materials research, and biophysics using ion beams from SIS200.

For atomic physics experiments with highly-charged, few-electron ions the cave will be equipped with a charge state spectrometer allowing for charge state separation

behind a reaction target for beam energies up to about 1 GeV/u (≈ 20 Tm). At such beam energies, life-time and precise photon and electron spectroscopy experiments will profit considerably from coincidence measurements with the final projectile charge state. Here, beam intensities of up to 10^9 ions/s are required. For atomic physics experiments at even higher beam energies of up to ≈ 20 GeV/u, e.g. resonant coherent excitation using channeling techniques, no charge state separation is foreseen and the desired beam intensity amounts to 10^8 ions/spill.

5.2.2 Experiments at NESR

Experiments at the Internal Jet Target

The interaction of cooled beams of high-Z ions with low-density gaseous matter provides the unique opportunity for a broad range of atomic collision and spectroscopy studies which are otherwise inaccessible. This is due to the high luminosity of the circulating ion beams on one hand and the almost background-free target environment on the other hand. For collision studies, representative examples are investigations of projectile inner-shell processes such as K-shell excitation/ionization, dynamically induced electron/positron production and the time-reversed processes of the most elementary atomic processes, i.e. photoionization or the Auger process. At the NESR it is planned to perform high resolution as well as kinematically complete differential studies of these processes by means of combined electron, photon, and recoil-ion momentum spectroscopy. For the case of atomic structure investigations, a prominent example for the advantage of using stored and cooled ion beams are the 1s-Lambshift studies for the case of H-like high-Z systems.

The Jet Target

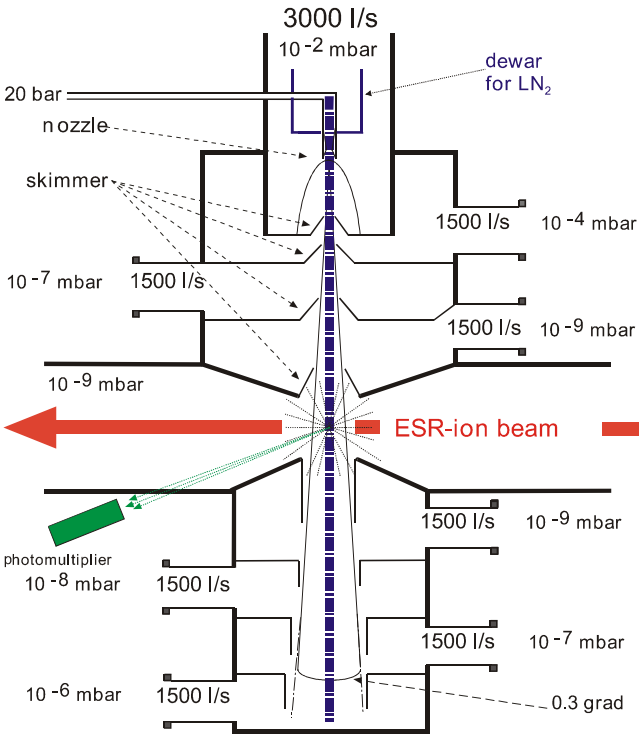

Figure 5.26: Schematic presentation of the ESR internal gas-jet target.

Therefore, the NESR will be equipped with a supersonic jet target similar to the one already in operation at the ESR (see Figure 5.26) with typical atom and cluster densities of 10^{12} to 10^{14} cm^{-3} [96]. In the jet-target chamber, the stored ions cross a perpendicularly oriented molecular or atomic supersonic gas-jet. The jet is produced by expanding a gas through a Laval nozzle. To meet the UHV requirements of the

ESR (≈ 10^{-11} mbar), the actual setup consists of an injection and a dump part, both separated by skimmers in four stages with a differential pumping system. The diameter of the gas-jet in the reaction chamber amounts to about 5 mm.

Low Energy Electron- and Recoil- Spectrometer

Processes with minimum momentum transfer **q** will in general constitute the dominant part of the total ionization cross section. So electrons with high multiplicity and low energy in their respective emitter frame and low-energy recoil ions constitute the overwhelming share of charged particles produced in these collisions.

In the standard configuration of the reaction microscope [3] a small longitudinal magnetic B-field and a longitudinal electric extraction E-field are generated around the target zone by a pair of Helmholtz coils and resistive potential plates, respectively. Low-energy electrons with an energy from few eV up to 1000 eV and recoil ions are extracted from the target zone and guided along the magnetic field lines onto 2D position-sensitive detectors which are positioned a few degrees from the primary beam direction. In experiments at relativistic velocities [97] the projectile ionization cross sections are typically a few barn. The electrons due to target ionization with a production cross section of about 10^{-15} cm^2 may overload these detectors. It is therefore important to remove the detectors for low-energy electrons and recoiling target ions from the direct view of the target zone. For this purpose a set of two large-aperture magnetic guiding systems for low-energy electrons and recoil ions, respectively, will be designed, e.g. to be used for studies of relativistic and QED effects in kinematically complete electron impact ionization of H-like U^{91+} [98].

Forward Electron Spectrometer

For high-resolution spectroscopy of electrons emitted in forward direction by the fast projectiles after direct ionization or autoionization, a magnetic spectrometer will be designed. It consists of a 60^0 dipole magnet, a quadrupole triplet followed by another 60^0 dipole and covers electron emission in a narrow cone around the projectile axis. Figure 5.27 displays the implementation of the forward electron spectrometer into the gas-jet area. In one mode of operation this spectrometer shall only momentum analyze electrons with high resolution and map them onto a detector. In another mode it permits that for electrons the collision plane and momentum and emission direction of all particles emerging from an ionization event is reconstructed by means of a two-dimensional, position-sensitive detector.

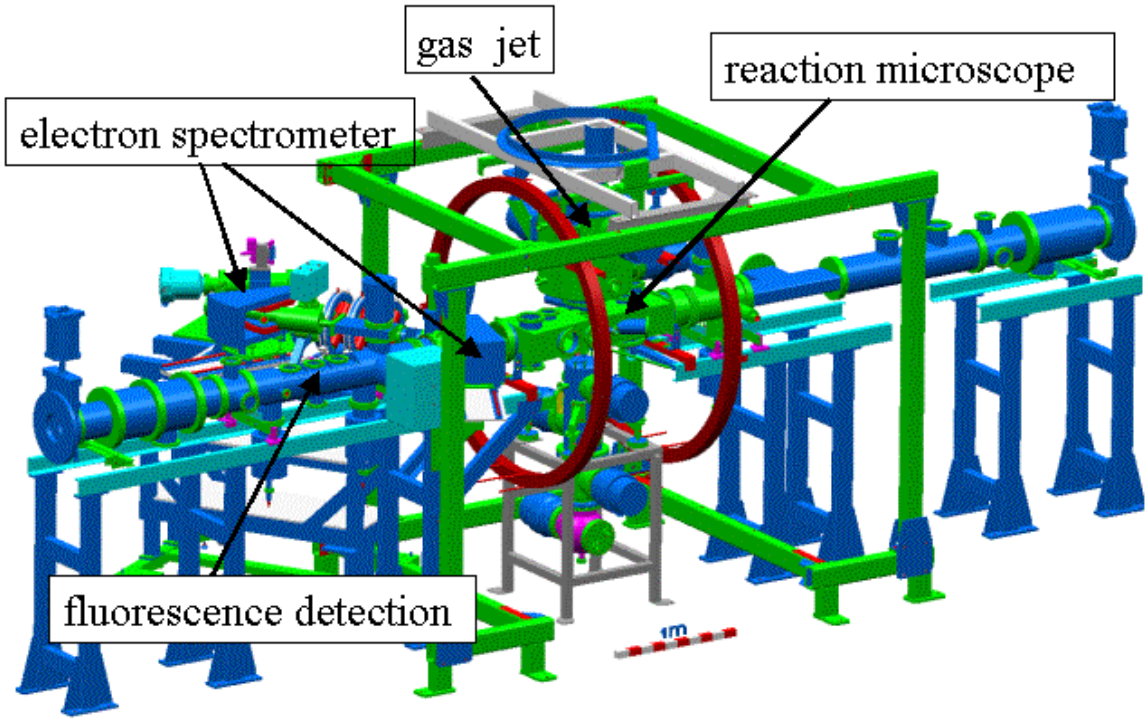

Figure 5.27: Experimental area at the supersonic jet target. The displayed jet environment comprises a recoil-ion reaction microscope, a zero-degree electron spectrometer and a device to detect fluorescence light emitted by laser-excited ions.

Photon Spectroscopy

The study of angular distributions and alignment or polarization effects for photon emission induced by atomic collisions will be addressed by a dedicated photon scattering chamber for the NESR jet target (see Figure 5.28). Here, also precision x-ray spectroscopy experiments on H-, He-, and Li-like high-Z ions will be conducted. This research will take advantage of new advanced detector devices such as μ-strip or calorimeter detectors currently under development.

Similar to the x-ray detection chamber at the ESR [99], the chamber will be equipped with various x-ray view ports allowing for a large angular range with respect to the ion beam axis. It is also planned to use the x-ray detection setup in combination with the reaction microscope and the forward electron spectrometer.

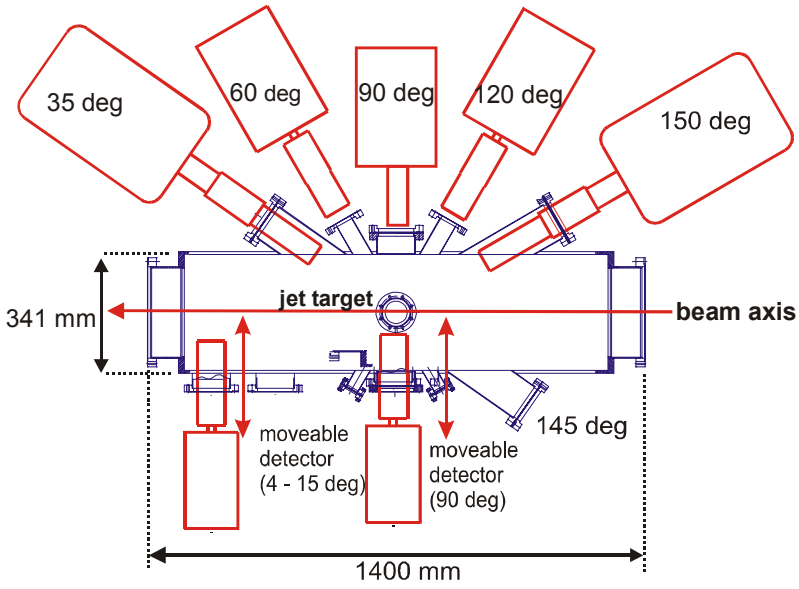

Figure 5.28: Photon detection area at the NESR jet target.

Experiments at the Electron Target

A series of studies of lithium-like high-Z ions was carried out at the ESR with the electron cooler serving as an electron target. Albeit successful, these studies revealed the disadvantages of the procedure: The cooler potential has to be switched repeatedly between the electron energy of interest and the cooling potential. Since the ion beam is not cooled during the measuring time, these times have to be only in the order of milliseconds, which limits the bandwidth of the relative electron-ion energies available to a few keV.

A storage ring equipped with a second electron target would allow even for dielectronic recombination (DR) studies of H-like uranium ions. In this case, the electron cooler can cool the ion beam, and can be used additionally for a fine-tuning of the ion energy. It was observed at the ESR that even a change of one Volt in the total cooler voltage of 150 kV leads to an observable shift of the Schottky noise signal of the ion beam. Planned studies of KLL dielectronic resonances of e.g. H-like Pb would then require less than 4 keV electron energy in the laboratory – a value that can be easily achieved with a second 'cooler-like' electron target.

The reason to choose an electron cooler as a second electron target is mainly its feasibility. An additional argument is the fact that it can be used to cool decelerated beams immediately after the RF deceleration and/or to render slow ejection after electron recombination possible.

The maximum high voltage of the electron target can be limited to comfortable 30 kV if the target can be rotated by 180° so that both parallel as well as counter propagating electron-ion collisions would be possible. For good luminosities, electron currents of up to 1 A have to be anticipated. The length of the cooler will be of the order of 5 meters. Since very cold electrons are of utmost importance, adiabatic

expansion cooling will be applied. Two straight sections for x-ray measurements under 0° and 180° before and after the cooler are foreseen. They will be equipped with rather large pockets for future x-ray detectors.

Laser Experiments

The ability to store a large number of ions over a wide range of highly-charged rare isotopes, together with the cooling capabilities makes the NESR an ideal instrument for precision laser spectroscopy. There will be two independent laser interaction regions available, where the laser and ion beams overlay over a distance of at least 5 meters, with control of the beam positions. For fluorescence detection a device of approximately 1.5 meter length will be sufficient (see Figure 5.27).

The generation of x rays with energies up to the MeV region is a very attractive additional possibility offered by the combination of an ultra-high intensity laser with the intense bunched electron beam foreseen at the NESR for the in-beam electron scattering experiments. As outlined in the theoretical paper by Esaray and coworkers [68], the requirements on the laser beam and the electron beam are high. The laser intensity in the interaction region must be above 10^{17} W/cm^2. The number of electrons within the interaction zone is determining the number of energetic backscattered photons. These γ rays can be exploited by studying their interaction with heavy ions in the storage ring if the following requirements are met:

- Electron bunches of less than 10 ps duration, less than 1 mm beam diameter, and more than 10^{12} electrons/bunch at energies between 30 MeV and 100 MeV.
- Ultra-high intensity laser (100 TW) with high repetition rate.
- Windows to allow laser pulses to be overlapped with the electron- and ion beams at the interaction zone. The window pointing head-on onto the electron beam has to be closer than 15 meters to the interaction point.
- Short bunches of radioactive isotopes in the NESR with more than 10^9 ions/bunch, cooled to beam diameters in the order of 1 mm.
- Detectors for positrons, electrons, photons, and particles.

The first item is within the parameter range of the accelerator proposed for electron scattering. The second item will already be fulfilled by the PHELIX laser presently under construction at GSI, except for a rather poor repetition rate. A common project with the Max Born-Institute aims at a repetition rate of better than 0.1 Hz, which is expected to be improved to several Hz within the next five years.

The detector requirements are mostly similar to those of a number of other experiments.

Experiments Using Extracted Ions from the NESR

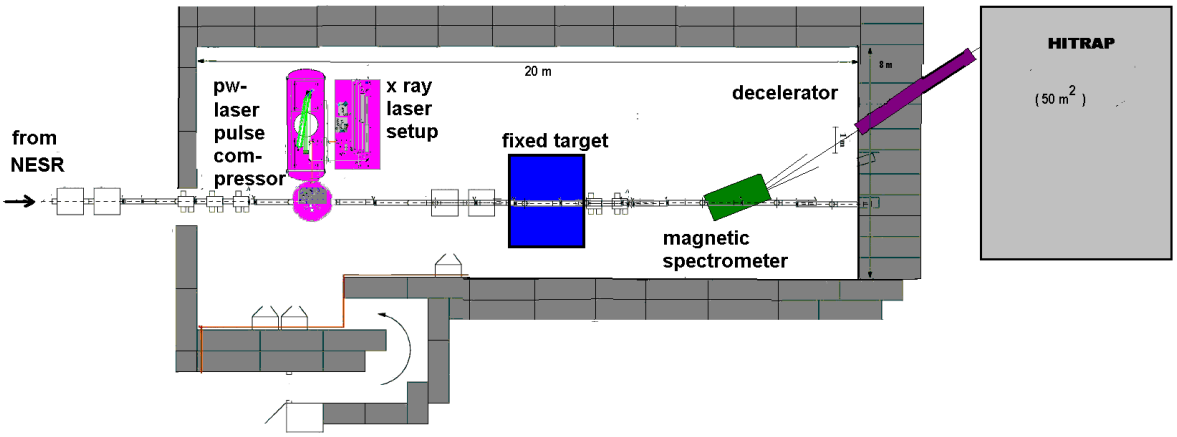

Figure 5.29: Atomic Physics area for experiments with extracted ion beams from the NESR. The facility will serve for different atomic physics experiments including petawatt (PW) laser interaction with highly-charged ions.

The availability of highly-charged heavy-ion beams, decelerated from a few hundred MeV/u even down to energies of about 3 MeV/u in the NESR offers the possibility to perform studies on exotic atomic systems. Besides in-ring experiments, investigations of systems far from ground-state charge equilibrium are of special interest for extracted ion beams. In particular:

- Surface/bulk interactions of slow, heavy ion beams (bare, H-, He- or Li-like) with different target materials.
- Hollow ion formation via interaction of heavy, highly charged projectiles with 'exotic' materials and structures, like fullerens, nanotubes and clusters.
- Spectroscopic studies of few-electron, heavy atomic systems including x-ray lasers.
- Interaction of slow, highly-charged ions with *electron gases* in a well defined structure (channeling).
- Interaction experiments with ultra-high intensity laser pulses.

The investigation of these processes requires the experimental access to different parameters of the collision partners (projectile, target) and other possible out-going interaction products (electrons, positrons and photons). The experimental setup will consist of large solid-angle spectrometers for reaction products.

The dedicated cave will contain a magnetic spectrometer for the charge-state separation of the projectiles after the interaction with the target (see Figure 5.29) with an ion momentum resolution of 10^3. For experiments to study the interaction of ions with pulses from the petawatt laser source PHELIX, the laser beam will be transported to the experiment. This requires re-imaging with evacuated spatially filtering telescopes. The equipment within the cave will contain the laser pulse compressor and an x-ray laser setup.

5.2.3 Trap Experiments with Highly-Charged Ions, Antiprotons, and Radioactive Atoms

HITRAP

A *trap facility* is planned for capturing and cooling of highly-charged ions or antiprotons produced at the future GSI-accelerator complex. A pilot facility will be HITRAP [20] to be installed at the present Experimental Storage Ring ESR. In the *HITRAP facility,* highly-charged, heavy ions will be available as bare nuclei (up to uranium U^{92+}), hydrogen-like ions or few-electron systems at low temperatures. Highly-charged ions are accelerated in the heavy-ion synchrotron, stripped in a foil to the desired charge state and injected into the storage ring NESR. For bare or hydrogen-like ions, energies of a few hundred MeV/u are required. In the NESR the ions will be decelerated to an energy of 3 MeV/u. They are then extracted in a fast-extraction mode as short ion bunches, decelerated and cooled to liquid helium temperatures in Penning traps.

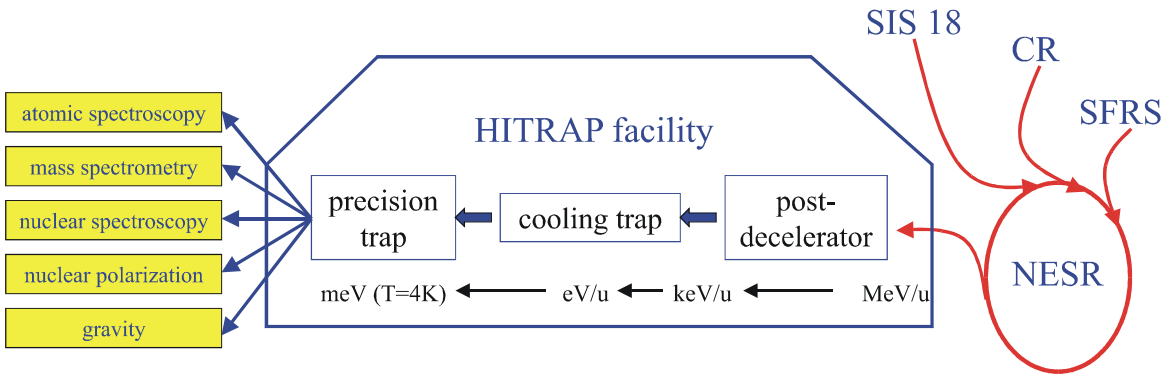

Figure 5.30: Scheme of the planned HITRAP facility. Highly-charged ions or antiprotons are extracted from the NESR storage ring, decelerated in a post-decelerator to ke -energies and then transferred into a Penning trap system.

With this novel technique of deceleration, trapping and cooling of highly-charged ions, atomic physics studies on slow HCI up to bare uranium interacting with photons, atoms, molecules, clusters, surfaces, and solids will be performed. In addition to collision studies, high-accuracy atomic physics experiments on trapped ions are part of the atomic physics program of the HITRAP facility at the ESR which will be conducted in a precision Penning trap.

The technological experience of deceleration, trapping and cooling of highly-charged ions, which will be gained at the ESR with the HITRAP facility, will be employed for a similar trap facility at the future storage ring NESR. The basic components constituting the new HITRAP facility are outlined in Figure 5.30. The high intensity of secondary beams produced at the Super-FRS will make it possible to extract decelerated radioactive ion beams from the NESR and to decelerate them for trap experiments with sufficient intensity. Therefore, the physics program at this *NESR trap facility* will focus on experiments with trapped radioactive ions and – eventually

– with trapped antiprotons. The facility will be placed behind the fixed target area (see Figure 5.29). An efficient re-bunching requires a distance of 40 m between the NESR extraction point and the decelerator.

After production, the highly-charged ions or antiprotons must be decelerated in the NESR and in a subsequent post-decelerator to energies of some keV/q (where q is the charge state of the ions) before catching, cooling and storing them in an ion trap. A final energy of the particles after deceleration in the NESR of 3 MeV/u is assumed. Two different post-deceleration techniques are being considered for the HITRAP project: an interdigital H-mode (IH) drift tube structure and a radiofrequency quadrupole structure (RFQ). Design parameters for an IH structure are given in Table 5.5.

Table 5.5: Parameters of a linear rf decelerator for the HITRAP facility.

Ion energy after extraction from NESR	3 MeV/u ($\beta \approx 0.080$)
Ion energy behind rf decelerator	≤ 10 keV/q
Ion mass-to-charge ratio	$A/q \leq 3$
Beam emittance behind NESR	$\varepsilon_{x,y} \leq 10\ \pi$ mm mrad
Pulse length behind NESR	≈ 1 μs
Beam emittance behind rf decelerator	$\varepsilon_{x,y} \leq 300\ \pi$ mm mrad
Ion beam diameter behind rf decelerator	≤ 10 mm
Beam intensity behind rf decelerator	some 10^6 ions/pulse (for U^{92+})
Resonator frequencies of IH structure	108 MHz

Highly-charged ions from the decelerator can be captured in a Penning trap at low energies with high efficiency. In a Penning trap charged particles are confined by a combination of a strong magnetic field and an electrostatic field which confines them in the direction parallel to the magnetic field lines. The Penning trap consists of a superconducting magnet and cylindrical electrodes to create the electrostatic trapping field. The cylindrical shape of the electrodes gives free access for the incoming ion beam. After capture the ions are cooled within less than one second in the trap and transferred to user experiments.

Neutral Atom Traps

Neutral radioactive atoms in traps are an ideal source for precise beta-neutrino (β-ν) correlation measurements, because the nuclei are confined in a well-defined volume without any supporting material. Recently, a collaboration at Los Alamos has reported on polarized radioactive nuclei (^{82}Rb-atoms) in a magnetic time-averaged orbiting-potential trap (TOP). This kind of trap allows for polarizing the nuclei via laser interaction. The Los Alamos group successfully measured the β-asymmetry parameter [53]. An important point is that the measurement of the β-ν correlation for

polarized nuclei gives access to the time-reversal violating parameters. Such measurements have not been attempted yet in traps. All collaborations active in this field are focusing on alkali elements which are ideal in terms of their simple electronic level scheme (optical pumping) and their chemical properties. With the installation of a neutral-atom trap at the Super-FRS facility, a variety of radioactive atoms not accessible at ISOL facilities will become available to such fundamental-interaction studies.

5.2.4 Experiments at HESR

Laser Experiments

The HESR provides electron cooling for relativistic ion beams up to $\gamma = 6$. This allows to extend precision spectroscopy with visible laser sources further into the regime of energetic transitions between inner shells. Using laser sources at 154 nm (fluor-excimer lasers), lithium-like 1s – 2p transitions can be excited in heavy ions up to the tin region. Transitions between metastable states populated in a gas target, and excited states with a fast branch to the ground state will be of special interest. The installations for such experiments will provide:

- A laser interaction region where the ion beam can be merged with the laser beam.
- Photon detection for the UV and soft x-ray region, photon detection over a length zone of about 1 meter.
- Space for laser installations (100 m^2), within 50 meters from the interaction zone in a radiation-free environment.

Experiments at the Internal Target

For atomic collision and spectroscopy studies an internal jet target such as discussed for the NESR (see chapter 5.2.2) is anticipated for the HESR. Note, that for bare uranium ions at $\gamma \approx 6$ colliding with a H_2-target the charge exchange is entirely governed by radiative electron capture (REC) and the reaction cross section amounts only to about 1 barn. Even for collisions with a Xe-target, the cross section increases moderately to about 50 barn. However, taking one- or few-electron ions into consideration, the reaction cross-section increases dramatically with target nuclear charge, e.g. from ≈ 30 barn for the case of H-like uranium colliding with H_2 to about 10 Kbarn for a Xe-target.

Photon Spectroscopy

For accurate photon spectroscopy of fast ions it is necessary to keep control over the observation geometry and thereby over the Doppler effects introduced. At zero degree observation one takes advantage of the relativistic forward boost of the intensity:

- The maximum Doppler shift.
- The relaxed requirements on angular accuracies.

Near zero degree the relative width $\Delta E_0/E_0$ of the photon energy in the emitter frame is for $\beta \approx 1$ approximately given by:

(5.9)

$$\left[\frac{\Delta E_0}{E_0}\right]^2 = \left[2\gamma^2 \left(\Delta\Theta_{Lab}\right)^2\right]^2 + \left[\frac{1}{\gamma}\Delta\gamma\right]^2 + \left[\frac{1}{E_x}\Delta E_x\right]^2$$

where the first term represents the contribution from the angular uncertainty. For the spectroscopy of Lyman-α photons of uranium which appear Doppler shifted from 100 keV to 1.2 MeV, an instrumental resolution ΔE_x of a Ge(i) detector corresponding to FWHM = 1.7 keV is assumed. This spectral width translates into 145 eV in the emitter frame of reference. According to equation (1) this width matches the angular Doppler width when the full opening angle of observation amounts to $\Delta\theta_{Lab} = 0.005$. This means a 10 mm diameter detector at a distance of 2 m. For the determination of the line centroid with a 100 times higher accuracy a correspondingly high positional stability of the system (including the gas-jet target) is required.

The favorable technical solution would be a segmented Ge(i) detector mounted in a pocket of the beam line downstream of the gas target. For the accuracy and count rates only the angular definition and the solid angle matters. Therefore, a detector could be moved a long way downstream if its size is correspondingly increased. Limitations arise only when the beam-line aperture is filled.

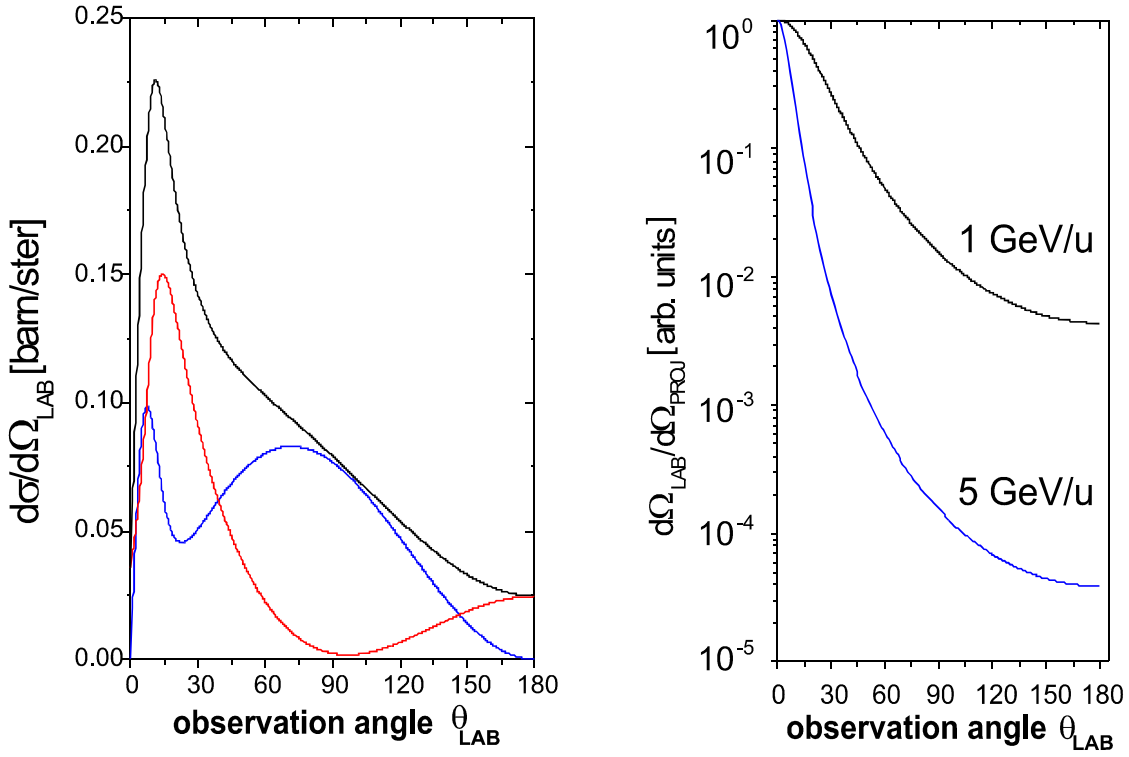

Figure 5.31: Left: Photon angular distribution for radiative electron capture into the K-shell of bare uranium ions at 5 GeV/u (blue line: electric contribution; red line: magnetic contribution) [2]. Right: intensity pattern of an isotropic projectile transition observed for 1 and 5 GeV/u in the laboratory.

In the case of REC into the K-shell of a high-Z projectile, a remarkable feature of the associated photon angular distributions is that the strong Lorentz boost of the x-ray intensity to forward observation angles is approximately cancelled by retardation effects, so that for beam energies up to 1 GeV/u deviations from a $\sin^2\vartheta_{LAB}$ pattern play a minor role. However, already at 5 GeV/u spin-flip contributions are predicted to

dominate completely the whole range of forward observation angles and even of backward observation angles which are larger than 120 deg. In Figure 5.31, the predicted angular distribution for K-REC in collisions of 5 GeV/u U^{92+} ions colliding with free electrons is depicted. This means that the K-REC radiation is detectable with a high differential cross section for the entire range of observation angles.

Electron Spectroscopy and Recoil Ion Momentum Spectroscopy

Among the high-γ experiments proposed, the dynamics of bound and free e^--e^+ pair creation and relativistic effects in quasi-photoionization of H-like very heavy ions can be addressed via electron impact ionization. Even the electron momentum dependence of QED effects is subject of experimental tests for the first time. In the following the requirements for electron and recoil spectroscopy at the supersonic jet target of the HESR are described.

For total positron production cross sections of typically close to one barn, a spectrometer covering a large solid angle is imperative. One goal of the experiment is to measure the probability for either process as a function of the impact parameter. The range of impact parameters for which discrepancies between perturbative and non-perturbative theories have been reported is below 100 fm, corresponding to projectile scattering angles of a few mrad. In this range, the impact parameters for a collision event can be derived best from the energy of the recoiling target ion. For this purpose a solenoidal B-field spectrometer is proposed which will allow to cover forward and backward cones of ± 75^0. It will be designed to measure electrons and positrons with energies up to 3 MeV and the associated angular distributions over the emission cones indicated. Recoiling target ions up to 1 MeV will also be transported by the instrument to the detector and resolved in energy by time-of-flight techniques.

Acknowledgment

This chapter, as all the other chapters of this document, was prepared with the help of many individuals. Appendix X lists the names of all the individuals involved in the CDR document, from the contributions to the science discussions, workshops and working groups to the research and development, the detailed scientific and technical planning activities, and, last not least, the drafting of this Conceptual Design Report.

The concepts and presentations of the science and technical plans in this chapter were in particular developed by the following authors:

Hartmut Backe, Fritz Bosch, Angela Bräuning-Demian, Siegbert Hagmann, Dorin C. Ionescu, Klaus Jungmann, Heinz-Jürgen Kluge, Gerhard Kraft, Christophor Kozhuharov, Thomas Kühl, Dieter Liesen, Paul H. Mokler, Reinhard Neumann, Wolfgang Quint, Sylvia Ritter, Dieter Schardt, Thomas Stöhlker, and Christina Trautmann

Collaborating Institutes and Contact Persons

• MPI für Kernphysik, Universität Heidelberg	D. Schwalm, J. Ullrich, A. Wolf
• HMI Berlin	J. Eichler
• MBI Berlin	W. Sandner
• TU Dresden	G. Soff
• Universität Frankfurt	R. Dörner, R. Dreizler, W. Greiner, H. Schmidt-Böcking
• Universität Gießen	A. Müller, E. Salzborn, K.-H. Schartner, W. Scheid
• Universität Greifswald	L. Schweikhard
• Universität Jena	E. Förster
• Universität Kassel	B. Fricke, S. Fritzsche
• Universität Mainz	H. Backe, G. Werth
• LMU München	D. Habs
• Universität Siegen	A.H. Walenta
• K.U. Leuven, Belgium	N. Severijns
• University of Jyväskylä, Finland	A. Jokinen
• LPC Caen, France	G. Ban
• CIRIL, GANIL Caen, France	H. Rothard
• SRF Grenoble, France	A. Simionovici
• IPN Lyon, France	D. Dauvergne, J.-C. Poizat

• CSNSM Orsay, France	D. Lunney
• GPS, Université de Paris, France	P. Indelicato
• Université de Paris, France	C. Cohen, J.P. Rozet, D. Vernhet
• University of Ferrara, University of Siena, Italy	R. Calabrese
• University of Cracow, Poland	Z. Stachura, A. Warczak
• University of Warsaw, Poland	K. Pachucki
• MSI, University of Stockholm, Sweden	R. Schuch
• CERN, Switzerland	J. Aystö
• KVI Groningen, The Netherlands	K .Jungmann, H. Wilschut
• St. Petersburg State University, Russia	L. Labzwoski, A.V. Nefiodov, V. Shabaev
• McGill University, Montreal, Canada	R. Moore
• IMP, Lanzhou, China	X. Cai, X. Ma
• RIKEN, Tokyo, Japan	Y. Yamazaki
• Argonne National Lab., USA	R.W. Dunford
• University of Berkeley, USA	R. Marrus, D. Schneider
• Kansas State University, Manhattan, USA	S. Hagmann
• Michigan State University, USA	G. Bollen

References

[1] For a comprehensive review on relativistic ion-atom collisions see J. Eichler and W. Meyerhof, Relativistic Atomic Collisions (Academic Press, San Diego, 1995)

[2] A. Ichihara, T. Shirai, J. Eichler, Phys. Rev.**A54** (1996) 4954

[3] J. Ullrich, R. Moshammer, R. Dörner, O. Jagutzki, V. Mergel, H. Schmidt-Böcking, L. Spielberger, J. Phys.**B30** (1997) 2917

[4] D.C. Ionescu and Th. Stöhlker, GSI Scientific Report, GSI 2001-1 (2001) 116

[5] W. Pieper and W. Greiner, Z. Phys.**218** (1969) 126

[6] L.D. Landau and E.M. Lifshitz, Sov. Phys.**6** (1934) 244

[7] R. Anholt and U. Becker, Phys. Rev.**A36** (1987) 4628

[8] U. Becker, N. Grün, W. Scheid, J. Phys.**B20** (1987) 2075

[9] H.F. Krause, C.R. Vane, S. Datz, P. Grafström, H. Knudsen, C. Scheidenberger, R.H. Schuch Phys. Rev. Lett.**80** (1989) 1190

[10] D.C. Ionescu and J. Eichler, Phys. Rev.**A54** (1996) 4960

[11] Th. Stöhlker, P.H. Mokler, F. Bosch, R.W. Dunford, B. Franzke, O. Klepper, C. Kozhuharov, T. Ludziejewski, F. Nolden, H. Reich, P. Rymuza, Z. Stachura, M. Steck, P. Swiat, A. Warczak, Phys. Rev. Lett.**85** (2000) 3109

[12] P.M. Mohr, G. Plunien, G. Soff, Phys. Rep.**293** (1998) 227

[13] PHELIX Project, GSI-98-10 Report, Dec. 1998

[14] H. Backe, GSI Workshop on its Future Facility (October 18-20, 2000)

[15] J. Schweppe, A. Belkacem, L. Blumenfeld, N. Claytor, B. Feinberg, H. Gould, V.E. Kostroun, L. Levy, S. Misawa, J.R. Mowat, M.H. Prior, Phys. Rev. Lett.**66** (1991) 1434

[16] H. Grotch and R.A. Hegstrom, Phys. Rev.**4** (1971) 59

[17] S.A. Blundell, K.T. Cheng, J.Sapirstein, Phys. Rev.**A55** (1997) 1857

[18] V. Shabaev, A.N. Artemyev, V.A. Yerokhin, O.M. Zherebtsov, G. Soff, Phys. Rev. Lett.**86** (2001) 3959

[19] H. Häffner, T. Beier, N. Hermanspahn, H.-J. Kluge, W. Quint, S. Stahl, J. Verdú, G. Werth, Phys. Rev. Lett.**85** (2000) 5308

[20] http://www.gsi.de/eurotraps/hitrap.htm

[21] C. Brandau, F. Bosch, G. Dunn, B. Franzke, A. Hoffknecht, H. Knoppe, C. Kozhuharov, A. Krämer, P.H. Mokler, A. Müller, F. Nolden, S. Schippers, Z. Stachura, M. Steck, T. Stöhlker, T. Winkler, A. Wolf, GSI-Scientific Report 1997, GSI-98-1 (1998) 104.

[22] T. Steih, W. Scheid, N. Grün, GSI-Scientific Report 1998, GSI-99-1 (1999), 103

[23] G. Audi, O. Bersillon, J. Blachot, A.H. Wapstra, Nucl. Phys.**A624** (1997) 1

[24] E.W. Otten, Nuclear Radii and Moments of Unstable Isotopes, Treatise on Heavy-Ion Science, **Vol. 8**, (ed.: D.A. Bromley, Plenum Publ. Corp., 1989) 517

[25] L.N. Labzowsky, A.V. Nefiodov, G. Plunien, G. Soff, D. Liesen, Phys. Rev. Lett.**84** (2000) 851

[26] For references on laser spectroscopy see: Proc. 1st Euroconference on "Atomic Physics at Accelerators: Laser Spectroscopy and Applications (APAC '99) ",

Sept. 1999, Mainz and Budenheim, Germany, ed. L. Schweikhard, H.-J. Kluge, Hyp. Int.**127** (2000)

[27] Ph. Bosselmann, U. Staude, D. Horn, K.-H. Schartner, F. Folkmann, A.E. Livingston, P.H. Mokler, Phys. Rev.**A59** (1999) 1874

[28] I. Klaft, S. Borneis, T. Engel, B. Fricke, R. Grieser, G. Huber, T. Kühl, D. Marx, R. Neumann, S. Schröder, P. Seelig, L. Völker, Phys. Rev. Lett.**73** (1994) 2425

[29] P. Seelig, S. Borneis, A. Dax, T. Engel, S. Faber, M. Gerlach, G. Huber, T. Kühl, D. Marx, K. Meier, P. Merz, W. Quint, F. Schmitt, M. Tomaselli, L. Völker, H. Winter, M. Würtz, K. Beckert, B. Franzke, F. Nolden, H. Reich, M. Steck, T. Winkler, Phys. Rev. Lett.**81** (1998) 4824

[30] K. Bailey, C.Y. Chen, X. Du, Y.M. Li, Z.-T. Lu, T.P. O'Connor, L. Young, in [26] p. 515

[31] G.D. Sprouse, J.S. Grossman, L.A. Orozco, M.R. Perason, in [26] p. 381

[32] H. Backe, A. Dretzke, M. Hies, G. Kube, H. Kunz, W. Lauth, M. Sewtz, N. Trautmann, R. Repnow; H.J. Maier, Hyp. Int.**127** (2000) 35

[33] C. Brandau, T. Bartsch, K. Beckert, C. Böhme, B. Franzke, A. Hoffknecht, H. Knopp, C. Kozhuharov, A. Krämer, P.H. Mokler, A. Müller, F. Nolden, S. Schippers, Z. Stachura, M. Steck, Th. Stöhlker; Th. Winkler, GSI-Scientific Report 1998; GSI-99-1 (1999) 90

[34] T. Steih, W. Scheid, N. Grün, private communication (1999)

[35] J. Dilling, D. Ackermann, J. Bernard, F.P. Hessberger, S. Hofmann, W. Hornung, H.-J. Kluge, E. Lamour, M. Maier, R. Mann, G. Marx, R.B. Moore, G. Münzenberg, W. Quint, D. Rodriguez, M. Schädel, J. Schönfelder, G. Sikler, C. Toader, L. Vermeeren, C. Weber, G. Bollen, O. Engels, D. Habs, P. Thirolf, H. Backe, A. Dretzke, W. Lauth, W. Ludolphs, M. Swetz and the SHIPTRAP Collaboration, Hyp. Int.**127** (2000) 491

[36] F. Herfurth, J. Dilling, A. Kellerbauer, G. Bollen, S. Henry, H.-J. Kluge, E. Lamour, D. Lunney, R.B. Moore, C. Scheidenberger, S. Schwarz, G. Sikler, J. Szerypo, Nucl. Instr. Meth.**A469** (2001) 254

[37] S. Schröder, R. Klein, N. Boos, M. Gerhard, R. Griesner, G. Huber, A. Karafillidis, M. Krieg, N. Schmidt, T. Kühl, R. Neumann, V. Balykin, M. Griesner, D. Habs, E. Jaeschke, D. Krämer, M. Kristensen, M. Music, W. Petrich, D. Schwalm, P. Sigray, M. Steck, B. Wanner, A. Wolf, Phys. Rev. Lett.**64** (1990) 2901

[38] J. Hangst, M. Kristensen, J.S. Nielsen, O. Poulsen, J.P. Schiffer, P. Shi, Phys. Rev. Lett.**67** (1991) 1238

[39] C.S. Wood, S.C. Bennett, D. Cho, B.P. Masterson, J.L. Roberts, C.E. Tanner, C.E. Wieman, Science **275** (1997) 1759

[40] V.A. Dzuba, V.V. Flambaum, I.B. Khriplovich, Z. Phys.**D1** (1986) 24

[41] G.D. Sprouse and L.A . Orozco, Ann. Rev. Nucl. Part. Sci.**47** (1997) 429

[42] L.N. Labzowsky, A.V. Nefiodov, G. Plunien, G. Soff, D. Liesen, Phys. Rev.**A63** (2001) 0054105

[43] P.G. Harris, C.A. Baker, K. Green, P. Iaydjiev, S. Ivanov, D.J.R. May, J.M. Pendlebury, D. Shiers, K.F. Smith, M. van der Grinten, P. Geltenbort, Phys. Rev. Lett.**82** (1999) 904

[44] E.D. Commins, S.B. Ross, D. DeMille, B.C. Regan, Phys. Rev.**A50** (1994) 2960; see also: E.A. Hinds and B.E.Sauer, Physics World **10** (1997) 37

[45] Workshop on "Nuclear Electric Dipole Moment", GSI-Darmstadt (November 1999) unpublished.

[46] R. Jaffe, hep-ph/0101280 (2001)

[47] I.B. Khriplovich and S.K. Lamoreaux, CP Violation without Strangeness (Springer, Berlin, 1997)

[48] Y.K. Semertzidis, in: Frontier Tests of Quantum Electrodynamics and Physics of the Vacuum, (Eds.: E. Zavattini, D. Baklanov, C. Rizzo 1998) 369

[49] K. Jungmann, NEDM workshop, GSI (1999)

[50] I.B. Khriplovich, Phys. Lett.**444** (1998) 98; I.B. Khriplovich, in: PANIC'99, (eds.: G.Fäldt, B. Höistad and S. Kulander, North Holland, 1999) p. 147c

[51] M.P. Bradley, Phys. Rev. Lett.**83** (1999) 4510

[52] F. Herfurth, J. Dillling, A. Kellerbauer, G. Audi, D. Beck, G. Bollen, H.-J. Kluge, D. Lunney, R.B. Moore, C. Scheidenberger, S. Schwarz, G. Sikler, J. Szerypo, and ISOLDE Collaboration, Phys. Rev. Lett.**87** (2001) 14 2501

[53] S.G. Crane, Phys. Rev. Lett.**86** (2001) 2967

[54] P. Delahaye, G. Ban, D. Durand, A.M. Vinodkumar, C. Le Brun, E. Liénard, F. Mauger, O. Naviliat, J. Szerypo, B. Tamain, Hyp. Int.**132** (2001) 475

[55] G. Savard, R.C. Barber, C. Boudreau, F. Buchinger, J. Caggiano, J. Clark, J.E. Crawford, H. Fukutani, S. Gulick, J.C. Hardy, A. Heinz, J.K.P. Lee, R.B. Moore, K.S. Sharma, J. Schwartz, D. Seweryniak, D.G. Sprouse, J. Vaz,, Hyp. Int.**132** (2001) 221

[56] D. Schneider, priv. communication (2001)

[57] Proc. 1st Euroconference on “Atomic Physics at Accelerators: Laser Spectroscopy and Applications (APAC ‘99) ”, Sept. 1999, Mainz and Budenheim, Germany (Eds.: L. Schweikhard, H.-J. Kluge) Hyp. Int.**127** (2000)

[58] M.A. Rowe, S.J. Freedman, B.K. Fujikawa, G. Gwinner, S.-Q. Shang, P.A. Vetter, Phys. Rev.**A59** (1999) 1869

[59] D. Beck, F. Ames, G. Audi, G. Bollen, F. Herfurth, H.-J. Kluge, A. Kohl, M. König, D. Lunney, I. Martel, R.B. Moore, H. Raimbault-Hartmann, E. Schark, S. Schwarz, M. de Saint Simon, J. Szerypo, D. Beck, Proposal to the ISOLDE Sci. Com., CERN/ISC99-13ISC/P111

[60] Z.-T. Lu, K.L. Corwin, K.R. Vogel, C.E. Wieman, T.P. Dinneen, J. Maddi, H. Gould, Phys. Rev. Lett.**79** (1997) 994

[61] S. Atutov, V. Biancalana, A. Burchianti, R. Calabrese, S. Gozzini, V. Guidi, P. Lenisa, C. Marinelli, E. Mariotti, L. Moi, K. Nasyrov, and S. Pod’yachev, Europ. Phys. J.**D13** (2001) 71 and private communication

[62] C. Wesdorp, F. Robicheaux, L.D. Noordam, Phys. Rev. Lett.**84** (2000) 3799

[63] E. Adelberger, B.R. Heckel, C.W. Stubbs, Y. Su, Phys. Rev. Lett.**66** (1991) 850

[64] K.B. Davis, M.-O. Mewes, M.R. Andrews, N.J. van Druten, D.S. Durfee, D.M. Kurn and W. Ketterle, Phys. Rev. Lett.**75** (1995) 3969; J.R. Ensher, D.S. Jin, M.R. Matthews, C.E. Wieman, E.A. Cornell, Phys. Rev. Lett.**77** (1996) 4984

[65] C.J. Myatt E.A. Burt, R.W. Ghrist, E.A. Cornell, C.E. Wieman, Phys. Rev. Lett.**78** (1997) 586

[66] T. Esslinger, MPQ Garching, private communication (2001)

[67] Th. Weber, M. Weckenbrock, A. Staudte, L. Spielberger, O. Jagutzki, V. Mergel, F. Afameh, G. Urbasch, M. Vollmer, H. Giessen, R. Doerner, Phys. Rev.**84** (2000) 443: R. Moshammer, B. Feuerstein, W. Schmitt, A. Dorn, C.D. Schroeter, J. Ullrich, H. Rottke, C. Trump, M. Wittmann, G. Korn, K. Hoffmann, W. Sandner, Phys. Rev. Lett.**84** (2000) 447

[68] E. Esarey, S.K. Ride, P. Sprangle, Phys. Rev.**E48** (1993) 3003

[69] Proceedings of the Fourth International Conference on Swift Heavy Ions in Matter (SHIM98), (Eds.:S. Klaumünzer, N. Stolterfoht , Berlin, 1998), Nucl. Instr. Meth.**B146** (1998)

[70] D.E. Groom, European Physical Journal **C15** (2000) 1

[71] C. Scheidenberger, H. Geissel, H.H. Mikkelsen, F. Nickel, T. Brohm, H. Folger, H. Irnich, A. Magel, M.F. Mohar, G. Münzenberg, M. Pfützner, E. Roeckl, I. Schall, D. Schardt, K.-H. Schmidt, W. Schwab, M. Steiner, Th. Stöhlker, K. Sümmerer, J. Vieira, B. Voss, M. Weber, Phys. Rev. Lett.**73** (1994) 50 and

C. Scheidenberger and H. Geissel, Nucl. Instr. Meth.**B135** (1998) 25

[72] H. Geissel and C. Scheidenberger, Nucl. Instr. Meth.**B136-138** (1998) 114

[73] H. Weik, H. Geissel, C. Scheidenberger, F. Attallah, T. Baumann, D. Cortina, M. Hausmann, B. Lommel, G. Münzenberg, N. Nankov, F. Nickel, T. Radon, H. Schatz, K. Schmidt, J. Stadlmann, K. Sümmerer, M. Winkler, H. Wollnik, Nucl. Instr. Meth.**B164-165** (2000) 168

[74] J. Mompart, C. Domingo, C. Baixeras, Nucl. Instr. Meth.**B107** (1996) 56

[75] C. Domingo, J. Font, C. Baixeras, Ll. Font, F. Fernández, Nucl. Instr. Meth.**B146** (1996) 114

[76] S. Datz, H.F. Krause, C.R. Vane, H. Knudsen, P. Grafström, R.H. Schuch, Phys. Rev. Lett.**77** (1996) 2925

[77] S. Datz, Nucl. Instr. Meth.**B164-165** (2000) 1

[78] J. Lindhard and A.H. Sørensen, Phys. Rev.**A53** (1996) 2443

[79] N.F. Shul'ga and V.V. Syshchenko, Nucl. Instr. Meth.**B164-165** (2000) 180

[80] A. Dadashev, M.P. Pasternak, G.Kh. Rozenberg, Rev. Sci. Instrum.**72** (2000) 2633

[81] S.A.T. Redfern and M.A. Carpenter (Eds.), Reviews in Mineralogy & Geochemistry, Vol. 39: *Transformation Processes in Minerals*, The Mineralogical Society of America, Washington, DC (2000)

[82] C. Trautmann, S. Klaumünzer, H. Trinkaus, Phys. Rev. Lett.**85**, 3648 (2000).

[83] G. Schiwietz, P. Grande, B. Skogvall, J.P. Biersack, R. Köhrbrück, K. Sommer, A. Schmoldt, P. Goppelt, I. Kádár, S. Ricz, U. Stettner, Phys. Rev. Lett.**69** (1998) 628

[84] G. Xiao, G. Schiwietz, P.L. Grande, N. Stolterfoht, A. Schmoldt, M. Grether, R. Köhrbrück, A. Spieler, U. Stettner, Phys. Rev. Lett.**79** (1997) 1821

[85] T. Kambara, Y. Kanai, T.M. Komjima, Y. Nakai, A. Yoneda, K. Kageyama, Y. Yamazaki, Nucl. Instr. Meth.**B164-165** (2000) 415

[86] K. Kimura, J. Kaneko, S. Sharma, W. Hong, N. Itoh, Phys. Rev.**B60** (1999) 12626

[87] S.B. Curtis and J.R. Letaw, Adv. Space Res.**9** (1989) (10)293

[88] J.R. Letaw, R. Silberberg, C.H. Tsao, Nature **330** (1987) 709

[89] J.W. Wilson, L.W. Townsend, W. Schimmerling, G.S. Khandelwal, F. Khan, J.E. Nealy, F.A. Cucinotta, L.C. Simonsen, J.L. Shinn, J.W. Norbury, Transport Methods and Interactions for Space Radiations, NASA Publication 1257 (1991)

[90] M. Krämer and G. Kraft, Radiat. Environ. Biophys.**91** (1994) 33

[91] G. Kraft, Nucl. Sci. Appl.**1** (1987) 3

[92] W. K. Weyrather, S. Ritter, M. Scholz, G. Kraft, Int. J. Radiat. Biol.**75**, (1999) 1357

[93] S. Ritter, E. Nasonova, G. Kraft, Proceedings of the 2nd International Space Workshop 2000, Chiba, NIRS/NASDA, 115-117

[94] S. Ritter S. Berger, T. Größer, P. Hessel, G. Kraft, E. Nasonova, K. Ando, E. Gudowska-Novak, GSI Scientific Report 2000, GSI-2001-1 (2001) 154

[95] T. Haberer, W. Becher, D. Schardt and G. Kraft, NIMB**A330** (1993) 296

[96] A. Krämer, A. Kritzer, H. Reich, Th. Stöhlker, Nucl. Instr. Meth.**B174** (2001) 205

[97] W. Nakel and C.T. Whelan, Physics Rep.**315** (1999) 409

[98] S. Keller, R.M. Dreizler, L.U. Ancarani, H. Ast, H.R.J. Walters, C.T. Whelan, Phys., Rev.**A59** (1999) 1284

[99] Th. Stöhlker, O. Brinzanescu, A. Krämer, T. Ludziejewski, X. Ma, P. Swiat, A. Warczak, AIP Conf . Proc. **506** (2000) 389